European Journal of Medicinal Chemistry 255 (2023) 115382

Contents lists available at ScienceDirect

European Journal of Medicinal Chemistry

journal homepage: www.elsevier.com/locate/ejmech

Review article

Small-molecule theranostics in Alzheimer's disease

Álvaro Sarabia-Vallejo, Pilar López-Alvarado, J. Carlos Menéndez *

Unidad de Química Orgánica y Farmacéutica, Departamento de Química en Ciencias Farmacéuticas, Facultad de Farmacia, Universidad Complutense, 28040, Madrid, Spain

ARTICLE INFO

Keywords:
Alzheimer's disease
Theranostic agents
β-amyloid protein
PET imaging
Optical imaging
Fluorescent probes

ABSTRACT

Alzheimer's Disease (AD) remains one of the most challenging health-related issues for our society. It is becoming increasingly prevalent, especially in developed countries, due to the rising life expectancy and, moreover, represents a considerable economic burden worldwide. All efforts at the discovery of new diagnostic and therapeutic tools in the last decades have invariably met with failure, making AD an incurable illness and underscoring the need for new approaches. In recent years, theranostic agents have emerged as an interesting strategy. They are molecules able to simultaneously provide diagnostic information and deliver therapeutic activity, allowing for the assessment of the molecule activity, the organism response and the pharmacokinetics. This makes these compounds promising for streamlining research on AD drugs and for their application in personalized medicine. We review here the field of small-molecule theranostic agents as promising tools for the development of novel diagnostic and therapeutic resources against AD, highlighting the positive and significant impact that theranostics can be expected to have in the near future in clinical practice.

1. Introduction

Dementia is a generic term describing a group of symptoms including cognitive impairment with memory decline, problem-solving difficulties, mood and behaviour alterations and daily-task performance hindrance. Among the multiple causes for dementia, Alzheimer's Disease (AD) holds the first place in terms of prevalence (60–80%), leading a list that also includes cerebrovascular disease (5–10%), frontotemporal lobar degeneration (5–10%), Lewy body disease (5%), hippocampal sclerosis and Parkinson's disease [1]. AD, one of the most common types of neurodegenerative diseases currently accounts for about 57 million cases worldwide and represents a considerable burden, especially, but not exclusively, in developed countries [2]. In 2050, AD is projected to exceed 150 million cases, attesting the substantial impact of this disease in our current and future society and making AD a devastating illness not only for patients, but also for their relatives and caregivers.

The clinical manifestations of AD involve memory loss with difficulty recalling recent information, mood alterations with depression and apathy, behavioural changes and other symptoms associated to cognitive impairment, leading in the later stages to physical disability with compromised walking and speaking and, finally, death. These manifestations tend to appear in a subtle manner during an extended period of time, where three phases are usually distinguished, namely preclinical AD (asymptomatic), Mild Cognitive Impairment (MCI, with slight symptoms not interfering with daily tasks) and Alzheimer's Dementia (symptoms start to interfere with daily performance with growing impact) [2]. The absence of symptomatology in the preclinical stage does not imply a lack of pathogenic mechanisms, which indeed can be observed as early as two decades prior to the onset of the symptoms, a fact that is highly significant in the search for tools for the early diagnosis of AD [3].

Even though the length of these stages is subject to individual variations, the progression of the disease is unavoidable, leading to changes in behaviour and personality and to an ever-increasing dependence for the most basic daily tasks.

Relentless research efforts notwithstanding, the aetiology of AD remains incompletely understood. Some processes are known to play a role in the onset and development of the disease, but it is not clear whether they are a cause or a consequence of the pathogenic mechanisms [1]. Protein misfolding leads to the formation and accumulation of aggregates that trigger neurodegeneration and neuronal death. β-Amyloid (Aβ) and tau proteins are the two main pathological hallmarks related to the development of AD, and both of them imply protein misfolding. Additional mechanisms, including oxidative stress, neuroinflammation, mitochondrial dysfunction and imbalances in cholinergic and glutamatergic tone, are also present in the progression of the

* Corresponding author.
E-mail address: josecm@farm.ucm.es (J.C. Menéndez).

https://doi.org/10.1016/j.ejmech.2023.115382
Received 7 March 2023; Received in revised form 12 April 2023; Accepted 14 April 2023
Available online 21 April 2023

Abbreviations

Aβ	Amyloid-β
AD	Alzheimer's Disease
AICD	APP intracellular domain
APP	Amyloid precursor protein
BBB	Blood-brain barrier
CSF	Cerebrospinal fluid
EMA	European Medicines Agency
FDA	U.S. Food and Drug Administration
^{18}FDG-PET	^{18}Fluorodeoxyglucose positron emission tomography
MCI	Mild cognitive impairment
MRI	Magnetic resonance imaging
NFT	Neurofibrillary tangles
NIA-AA	National Institute on Aging and Alzheimer's Association
NIR	Near-infrared
PBS	Phosphate buffered saline
PET	Positron emission tomography
PHF	Paired helical filaments
PHTZ	Phenothiazine
PiB	Pittsburgh compound-B

disease. Some risk factors are associated with the appearance of AD, such as intrinsic factors like ageing, genetic factors (genes related to amyloid precursor protein APP, γ-secretase – PSEN1 and PSEN2 – and apolipoprotein E, among others), medical conditions (cardiovascular disease, traumatic brain injury, infections, diabetes, obesity) and external factors such as environmental exposure to metals – aluminium, lead, cadmium – and lifestyle-related factors (unhealthy diets, smoking) [1,4,5].

Previous reviews highlighted the relevance of the search of novel therapeutic [6–8] and diagnostic [9–13] approaches against AD, but the theranostic angle has been reviewed with the focus placed on nanotherapies [14–16]. The present article provides a critical review of the most relevant advances in the development of small-molecule theranostic agents against AD.

2. Protein deposition in Alzheimer's disease

2.1. Amyloid-β deposition

The processing of amyloid precursor protein (APP), a transmembrane protein involved in synaptogenesis and other synaptic functions, can follow two different pathways.

(a) Through the non-amyloidogenic route, APP is cleaved first by ***α***-secretase and then by ***γ***-secretase into sAPP***α*** and p3 proteins, which are released to the extracellular environment, and the APP intracellular domain (AICD), which is able to translocate to the nucleus for gene expression regulation [1,17,18].
(b) Through the amyloidogenic pathway, APP is cleaved, first, by β-secretase, and then by ***γ***-secretase, to release sAPPβ and amyloid-β (Aβ) proteins to the extracellular media, and AICD. Aβ peptides ranging from 43 to 51 amino acids are further processed in endocytic compartments after temporary internalization, giving rise to the two extracellular main forms of Aβ, containing 40 and 42 amino acids of, respectively, and known as $A\beta_{40}$ and $A\beta_{42}$ [18]. $A\beta_{40}$ is the most abundant species in the brain and $A\beta_{42}$ is the most aggregation-prone form, involved in nucleation and seeding [19]. The $A\beta_{42}$:$A\beta_{40}$ ratio in cerebro-spinal fluid (CSF) decreases in early AD, and is used as a valuable biomarker [19,20].

Aβ monomers tend to aggregate through nucleation forming oligomers, protofibrils and highly ordered fibrils with cross-β structure [21]. In a larger scale, the assembly of fibrils into plaques represents the last step of amyloid-β deposition. Soluble monomers and oligomers (aggregates of two to twelve monomers) are known to be the most neurotoxic species *via* the induction of mitochondrial dysfunction, calcium signalling disruption, hyperactivation of glutamate receptors and increased oxidative stress [19,22,23]. Furthermore, plaque-preceding Aβ oligomer-dependent neuronal hyperactivity is considered to contribute to the system dysfunction present at early stages of AD, supporting the consideration of monomers and oligomers as the primary causing agents of the disease [19,23]. Thus, efforts in the search for a valid therapeutic target have shifted in recent years from the insoluble fibrils and plaques, thought to be essentially inert and able to serve as a store of excess amyloid, towards these soluble forms. In this connection, it is thought that apolipoprotein E helps keeping Aβ clustered into plaques rather than toxic oligomers, which can be considered a neuroprotective response [24]. This conclusion is reinforced by the observation that blocking the expression of apolipoprotein E in APP transgenic mice results in plaque disruption and liberation of toxic Aβ oligomers [24].

The role of microglia in Aβ deposition is complex. On one hand, physiological mechanisms involving microglia and astrocytes contribute to stop the growth of amyloid-β plaques and remove them. Microglia is able to migrate to the surroundings of Aβ plaques to prevent the recruitment of more Aβ peptide [25]. Microglia also performs the clearance of Aβ through the secretion of degrative enzymes and the internalization of fibrils, but its capacity is limited and diminishes with ageing [21]. On the other hand, inflammation induced by activated microglia can also cause fibril formation [26].

Amyloid-β deposition is widely considered as one of the main pathological hallmarks of the early onset of AD, being present as soon as 20 years before the first symptoms show up, and its ability to trigger and spread synaptic damage, neurodegeneration and tau pathology render it an attractive target for early-stage treatment and diagnosis [3,19]. The factors causing the transition from Aβ homeostasis to the accumulation of misfolded Aβ oligomers due to imbalances in the formation and clearance of Aβ are still unknown [27].

2.2. Tau protein deposition

Tau protein is a microtubule-associated protein that is involved in the stabilization and modulation of microtubules and plays a critical role in axonal transport and growth and neuronal polarization. Tau phosphorylation and dephosphorylation regulates its binding to microtubules. Under pathological conditions, tau is hyperphosphorylated and aggregates into paired helical filaments (PHF) and further into neurofibrillary tangles (NFT), leading to neuronal dysfunction and death [28]. Aggregation of tau protein is a pathological hallmark in AD and is also under study for its potential as a therapeutic and diagnostic target.

3. Diagnosis of Alzheimer's disease

Diagnostic methods for AD are scarce and rather limited in their scope. Available diagnostic tools provide a useful guidance, but are not able to confirm unequivocally the presence of AD, which can only be achieved in *post mortem* histopathological studies. The development of methods to accurately diagnose AD, especially in the early stages, is key in the search for effective therapies, since one of the main drawbacks of current research in this area is that the administration of a treatment when the disease is too advanced does not allow to properly assess its effectiveness. Beyond patient and family history and cognitive and functional assessments, which have been widely used to establish a diagnose, structural imaging and biomarker measurements are becoming routine diagnostic tools against AD, even though it is still not clear in which order to perform this type of tests [29]. The discovery of biomarkers in blood, urine, saliva and, specially, cerebrospinal fluid (CSF),

and the use of magnetic resonance imaging (MRI) to study the morphology and volume of the brain, the atrophy of regions and the relationship between grey and white matter [30] is of special relevance. Neurodegeneration can be assessed by MRI and ^{18}fluorodeoxyglucose positron emission tomography (^{18}FDG-PET), but it is not as reliable as amyloid and tau detection for the early diagnosis of AD since neurodegeneration usually occurs years after the deposition of misfolded proteins has damaged the brain.

3.1. Magnetic resonance imaging (MRI)

Measuring the volume of the brain and ventricles and the atrophy of certain regions provides useful information for the evaluation of neurodegeneration. Medial temporal lobe atrophy is highly correlated to AD neurodegeneration and is evaluated through MRI [29]. This technique measures the progress of atrophy, which is closely related to cognitive impairment, and it is safe and widely employed [31]. Nevertheless, MRI is not able to confirm the diagnosis of AD.

3.2. ^{18}FDG-PET

There is strong evidence that hypometabolism of posterior cingulate and temporoparietal regions is a sign of neurodegeneration in AD, and it can be evaluated with the ^{18}F-labelled glucose derivative in ^{18}FDG-PET [29]. Despite the fact that this is a highly specific and sensitive technique able to predict AD risk and evolution according to metabolic patterns in relatively advanced stages of AD, its use is not widespread [31]. Furthermore, the use of a radiolabelled tracer with a short half-life (109.7 min) makes it necessary to prepare the probe in a cyclotron right before its administration. There is also increasing evidence that this technique provides information about glucose consumption not only by neurons but also by microglia, and in fact it is believed that ^{18}FDG-PET provides a better diagnosis of microglia activation than of neuronal functionality [32].

3.3. Amyloid-PET imaging

Amyloid-β deposition in the cortical region can be observed through amyloid-PET imaging, allowing to discard AD if amyloid-β is not present. Thus, amyloid-β is the earliest biomarker in AD, but there is not a clear correlation between plaque deposition and the severity of the disease, especially in later stages [31]. The first promising amyloid radiotracer, known as Pittsburgh compound-B (PiB) (Fig. 1), is a radioactive ^{11}C probe inspired in the thioflavin T dye that can differentiate AD from other dementias like frontotemporal dementia, distinguishes among the stages of AD and has a higher diagnostic value when combined with ^{18}FDG-PET [33–35]. For these reasons, PiB has been widely used to monitor the anti-amyloid activity of drug candidates in clinical trials. Nonetheless, this compound has some drawbacks since it is aimed mainly to fibrils and binds only weakly to soluble Aβ, and it has

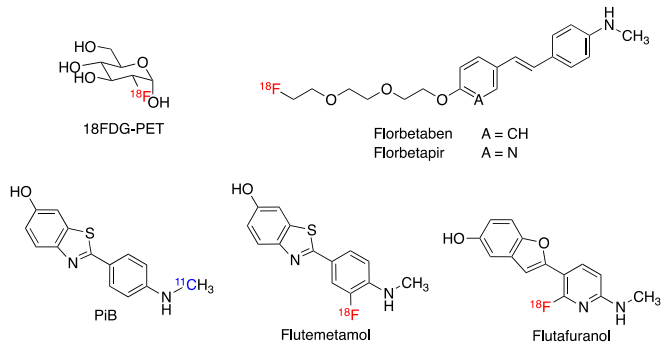

Fig. 1. Hypometabolism (^{18}FDG-PET) and amyloid PET tracers for the diagnosis of AD.

a short half-life (20 min), making necessary to have a cyclotron in the medical centre. Moreover, a positive with this technique is poorly selective [36–38].

To overcome the short half-life of PiB, ^{18}F-radioligands were developed and are used as a complementary tool in the diagnosis of AD, but not as a final confirmation of the disease [39]. To date, there are three such tracers currently approved by the EMA and the FDA: florbetaben, florbetapir, and flutemetamol. Florbetaben was the first ^{18}F-radioligand and, like florbetapir, it is inspired in the structures of dyes such as Congo Red and Chrysamine G Aβ [39]. Flutemetamol is, like PiB, a derivative of thioflavin T [39]. Although there are not significant differences among their diagnostic accuracies, ^{18}F-radioligands show a higher non-specific binding to the white matter than PiB due to their higher lipophilicity, producing more background noise [39,40]. A novel ^{18}F-radioligand, ^{18}F-NAV4694 or flutafuranol, developed as an analogue of PiB, showed similar cortical distribution to that of PiB and lower non-specific binding to the white matter than previous ^{18}F-radiotracers [41].

Although this first generation of PET tracers has improved the diagnosis of AD, they have important limitations, such as the complexity of their synthesis coupled to the urgency of their usage after the radioisotope preparation, the difficulties found in data analysis, the limited availability of suitable scanners and the fact that these probes can only detect amyloid aggregates around 5 years before the clinical syndrome starts and are not able to detect soluble Aβ forms [42].

3.4. Tau-PET imaging

Considering that most anti-Aβ drugs have failed in clinical trials and that tau protein aggregation is more closely related to the clinical progression of AD, particularly in advanced stages, in recent years many researchers have focused on the development of tau-PET radiotracers [39]. There is also evidence that in the first stages of AD Aβ oligomers and tau accumulation products different from neurofibrillary tangles (NFTs) are responsible of the toxicity and neurodegeneration rather than the Aβ plaques and NFTs [39]. ^{18}F-FDDNP (Fig. 2) was the first tau-PET radioligand, although it could also bind to Aβ due to the shared β-sheet conformation between Aβ and tau aggregates [31]. The ^{11}C-PBB3 tracer can detect tau protein in AD but also in other tauopathies, and has a higher binding affinity for tau than to Aβ [43]. Some inconvenience is caused by its short half-life (20 min) and by the fact that its principal metabolite is also able to cross blood-brain-barrier (BBB) [44]. Benzimidazole and quinoline derivatives BF-126, BF-158/^{11}C–BF-158 and BF-170 were the first selective tau-PET tracers. They showed excellent brain uptake and rapid clearance from normal brain tissue when administered to healthy mice, as well as the capacity to mark NFT in AD brain sections [45]. Further research led to the design and synthesis of ^{18}F-THK5105 and ^{18}F-THK5117, which bind to PHF-tau with affinity and selectivity over Aβ and are suitable for *in vivo* application, but display non-specific binding to the white matter due to the presence of myelin β-sheet conformation [46–48]. To avoid this problem, the arylquinoline ^{18}F-THK5351 was developed. This compound is efficiently cleared from the white matter and its binding correlated with tau deposition in human brain, and demonstrated faster kinetics and higher contrast than ^{18}F-THK5117 [49]. These findings make ^{18}F-THK5351 a promising tau-PET ligand. Flortaucipir (^{18}F-T807, ^{18}F-AV1451) and ^{18}F-T808 demonstrated both good affinity and selectivity towards tau protein over Aβ, a good brain uptake and a rapid washout [50]. However, ^{18}F-T808 experienced defluorination *in vivo* with subsequent ^{18}F uptake by the skull bone [51]. Flortaucipir showed a distribution consistent with that of tau protein in AD. Flortaucipir received FDA approval in 2020.

3.5. Cerebrospinal fluid (CSF) biomarkers

CSF biomarkers are very convenient diagnostic tools due the ease and promptness of their obtention and study, but there is still much

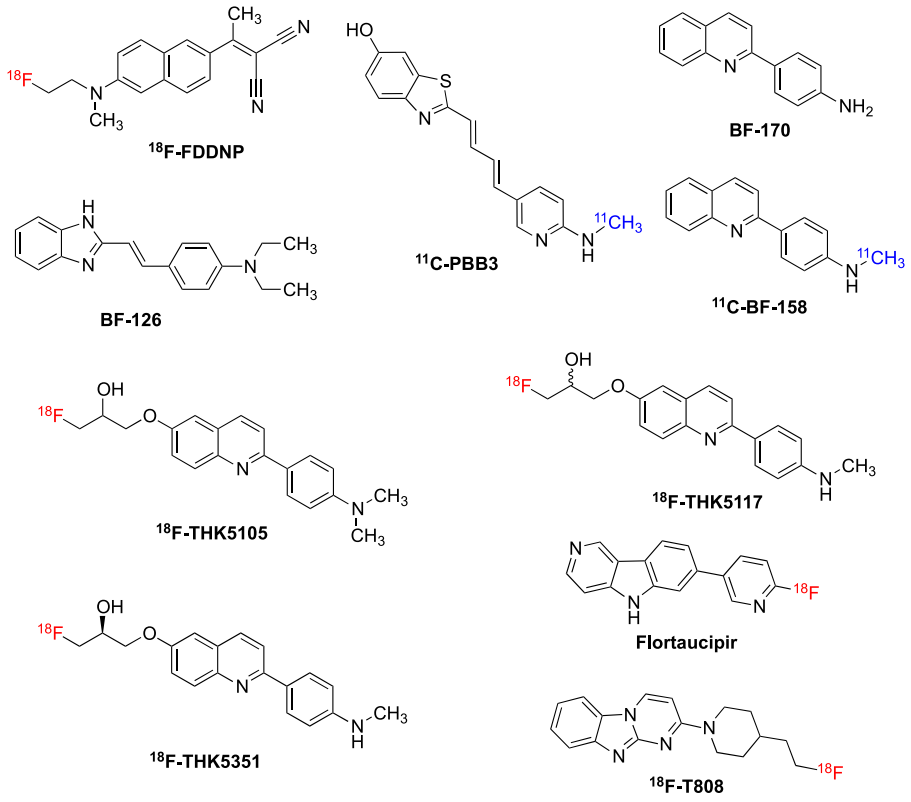

Fig. 2. Tau PET tracers for the diagnosis of AD.

research to perform to make them a more accurate and reliable method for the diagnosis of AD. The use of several biomarkers at the same time as a composite biomarker is thought to be the best manner to efficiently diagnose AD [30]. $A\beta_{42}$ is the Aβ form most prone to seeding and forming aggregates, thus being less available as soluble monomers during the course of AD; this is the explanation for the strong correlation found between low $A\beta_{42}$ levels in CSF and significant Aβ plaques in the brain [19,52]. Nevertheless, the $A\beta_{42}$:$A\beta_{40}$ ratio provides a more accurate image of the progression of AD and is regarded, together with the level of $A\beta_{42}$ in CSF, as one of the reference biomarkers to direct the diagnosis of AD in the recently updated guidelines from the National Institute on Aging and Alzheimer's Association (NIA-AA) [20,53]. Tau detection in CSF, either the total tau protein or only phosphorylated tau protein, are also reliable biomarkers for the diagnosis of AD and are established by this organization as a reference in the framework of the diagnosis of AD [20,54].

3.6. Retinal imaging

Both $A\beta_{40}$ and $A\beta_{42}$, Aβ aggregates, tau protein and NFT have been detected in the retina of AD patients and proven to show correlation with the presence of the disease, making this a non-invasive and easy to access potential technique to diagnose AD [55,56]. Nevertheless, more studies are needed to strengthen the evidence.

4. Treatment of Alzheimer's disease

Currently, there is no cure for AD in spite of extended research efforts. Commercially available drugs only achieve a temporary relief of the symptoms, but do not cure nor stop the advancement of the disease. Acetylcholinesterase inhibitors, a NMDA receptor antagonist and two anti-amyloid monoclonal antibodies are the only approved drugs against AD.

4.1. Small-molecule therapies

Due to the death of cholinergic neurons, AD is associated with cholinergic deficiency. By inhibiting acetylcholinesterase, these drugs restore acetylcholine levels, with the consequent symptomatic amelioration. There are three orally administered drugs in this group, namely rivastigmine, galantamine and donepezil (Fig. 3). While donepezil and galantamine are rapid-action reversible acetylcholinesterase inhibitors, rivastigmine is a slow-action reversible inhibitor of both acetyl- and butyrylcholinesterase [57]. A transdermic formulation of rivastigmine is also available, which may enhance adherence to the treatment. Tacrine was also an acetylcholinesterase inhibitor used against AD, but due to hepatotoxicity issues it is no longer used in clinical practice [58].

Memantine is an antagonist of the NMDA receptor, working as a partial antagonist with moderate affinity, strong voltage-dependency and fast kinetics (Fig. 3). As a consequence, the pathological increase of glutamate is quenched by the blockade of the channel and intracellular calcium accumulation is slowed [57]. It is orally administered and can be combined with acetylcholinesterase inhibitors, resulting in an improvement of the state of the patients, usually with additive effects and with no increase in adverse effects [59].

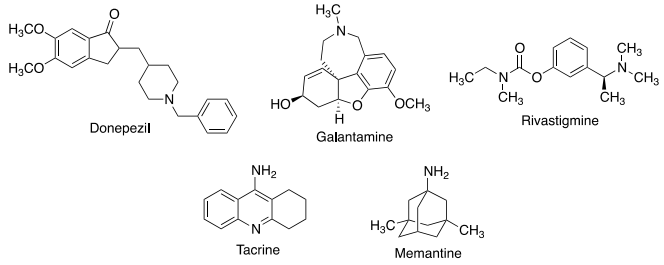

Fig. 3. Small-molecule treatments of AD.

4.2. Anti-amyloid monoclonal antibodies

Aducanumab is a IgG1 monoclonal antibody targeting Aβ soluble oligomers and insoluble fibrils [60,61], and is thus considered the first drug aimed towards one of the causes of Alzheimer's disease. Aducanumab decreases amyloid plaques and, in a small subset of patients, showed a reduction of phosphorylated tau in CSF and medial temporal NFT [62]. Not exempt of controversy, the clinical efficacy and safety of aducanumab in AD has been questioned [63] and, while the FDA approved the drug and considered it a first-in-class medication, the EMA rejected it. Due to the very high rate of serious adverse events, caution is required in its clinical use [64].

Lecanemab is a humanized IgG1 monoclonal antibody that binds with high affinity to amyloid-β soluble protofibrils [65]. It has been shown to moderately slow mild cognitive decline and reduce amyloid-β plaques in patients with early Alzheimer disease and has recently gained accelerated approval for this indication from the FDA.

4.3. Shortcomings of conventional drug discovery for Alzheimer's disease

Past efforts at the discovery of anti-Alzheimer drugs were valuable but missed key aspects of the disease course, progression and pathological processes, which can explain the repeated failures in clinical trials of diverse drug candidates aimed at varied different targets and operating by diverse mechanisms. Thus, in the past years, many promising drug candidates failed in their way to approval, including the anti-Aβ agents semagacestat, bapineuzumab and solanezumab, β-secretase inhibitors lanabecestat, verubecestat and atabecestat, γ-secretase inhibitors semagacestat, avagacestat and tarenflurbil (with significant adverse effects), α-secretase modulators such as etazolate, which promotes the non-amyloidogenic route mediated by α-secretase through the modulation of the GABA receptor, metal chelators and many antibodies [59,66]. The reasons for this failure are not unique, but probably arise from a combination of the following: (a) the poor understanding of the disease and its causes; (b) the long preclinical phase without symptoms but with key underlying pathological mechanisms; (c) administration in a late stage of the disease after surpassing key thresholds; (d) attempting to address the problem with single-target molecules; (e) the lack of homogeneity of the populations of study; (f) the limited diagnosis ability and (g) the lack of clear biomarkers for the classification of the patients [59].

This scenario calls for the introduction of novel approaches in the search for diagnostic tools and therapeutic agents against AD and other neurodegenerative diseases.

5. Theranostic compounds for Alzheimer's disease

5.1. Introduction to theranostics

Theranostic agents can be defined as molecules able to provide diagnostic information and therapeutic activity at the same time. The long-term goal of theranostics is to gain the ability to provide early diagnosis and fine-tuning of therapy with a degree of control that is unattainable with current therapeutic tools, paving the way to truly personalized medicine. This approach allows assessment of the activity of the molecules under study, the response of the organism to them and their pharmacokinetics, giving information that can contribute to the research stage and also to clinical practice. As an additional benefit, this approach will lead to a better understanding of the fundamental mechanisms that constitute risk factors able to trigger the development of the disease (Fig. 4). Amyloid fibrils may be considered both as a therapeutic target and as a neuropathological hallmark in a variety of neurodegenerative diseases, and are therefore a suitable target for a theranostic approach. Importantly, the brain deposition of Aβ precedes clinical symptoms by several years, making *in vivo* imaging of Aβ particularly suitable for identifying individuals at risk and in the early stages of AD. This approach seems useful considering that the failure of Alzheimer drug candidates has been attributed to their administration at a late stage, when the pathology is too advanced. Therefore, early diagnosis and disease monitoring appear to be critical for an efficient therapy, and these issues can be addressed with the theranostic strategy.

There are several types of chemical entities with potential theranostic activity against AD. In this review, recent advances in the field of conventional small-molecule theranostic agents against AD will be discussed, although other advances can be pointed out in additional areas such as nanoparticles [15], nucleic-acid based therapies [67] and peptides [68].

5.2. Initial optical imaging-based theranostic agents targeting Aβ

The near-infrared (NIR) region of the electromagnetic spectrum (NIR-I region) spans from 650 to 950 nm, and its use in biomedical imaging has many advantages as a biological window thanks to its adequate penetrability and reduced autofluorescence causing small background noise in biological tissue, its non-invasiveness and its innocuousness [69].

Many candidate probes for AD diagnosis are derived from the structure of amyloid dyes like thioflavin T or Congo red (Fig. 6), both of which are able to bind to Aβ due to their ability to intercalate in the β-sheet structure. Even though the initial interest in these compounds was focused primarily on their ability to bind and mark Aβ, some of them, such as Congo red and its analogue chrysamine G, also showed therapeutic potential through Aβ-aggregation inhibition activity [70–72].

Thioflavin T is an amyloid dye exhibiting fluorescence emission in the visible range, with a noticeable increase in the fluorescent intensity upon amyloid binding [73]. Thioflavin T displays a significant shift in both the excitation and emission maxima towards longer wavelengths of its fluorescent emission upon binding [74]. As a drawback, Thioflavin T bears a positive charge, leading to poor permeability across the blood-brain barrier (BBB) [72]. For this reason, several thioflavin T

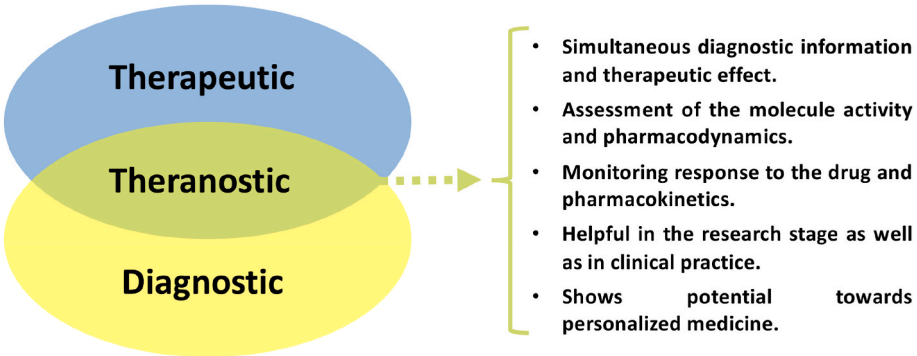

Fig. 4. Some advantages of the theranostic approach.

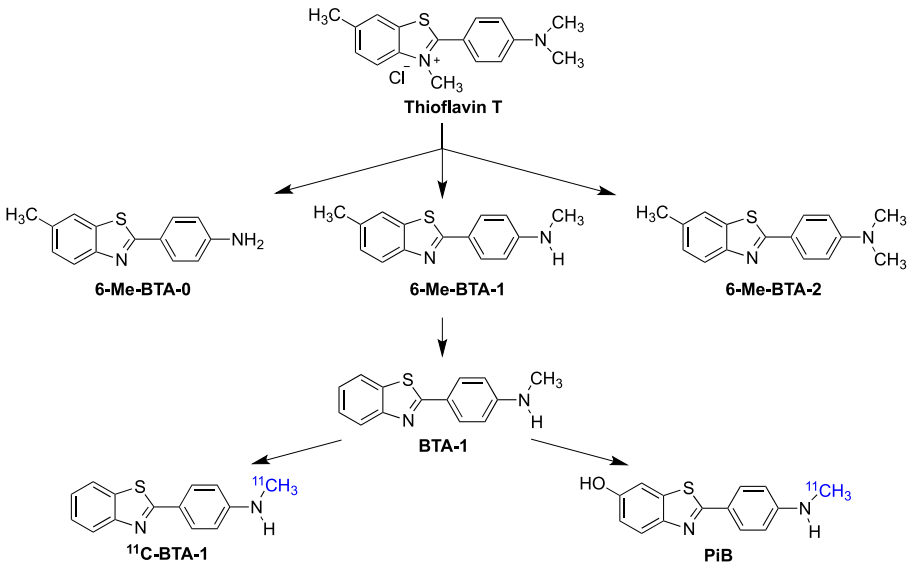

Fig. 5. Design of BTA-1 and PiB from thioflavin T.

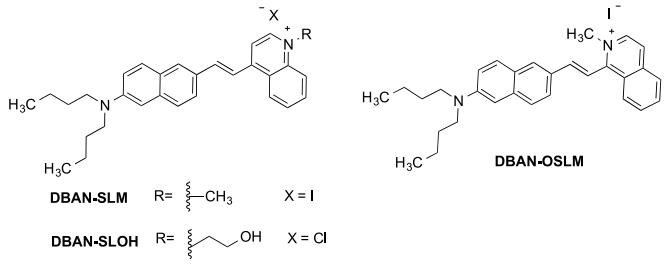

Fig. 9. Structures of naphthylamine-derived cyanine theranostic agents against AD.

derivatives with increased lipophilicity (6-Me-BTA-0, 6-Me-BTA-1 and 6-Me-BTA-2) were developed and shown to be able to stain amyloid plaques as well as neurofibrillary tangles in brain slices, as revealed through fluorescence microscopy. Unfortunately, 6-Me-BTA-1, the only candidate evaluated for its fluorescence upon amyloid binding *in vitro*, did not display shifts in their excitation and emission maxima wavelengths following amyloid binding [75]. Labelled derivatives of these compounds were also employed for PET imaging. Thus, the administration of ^{11}C-BTA-1, a radioactive derivative lacking the methyl residue in position 6 of benzothiazole, resulted in high brain uptake, and imaging of amyloid deposits was verified by multiphoton microscopy for its non-labelled analogue BTA-1 [76]. The hydroxylation of position 6 of benzothiazole in ^{11}C-BTA-1 resulted in the compound called Pittsburgh

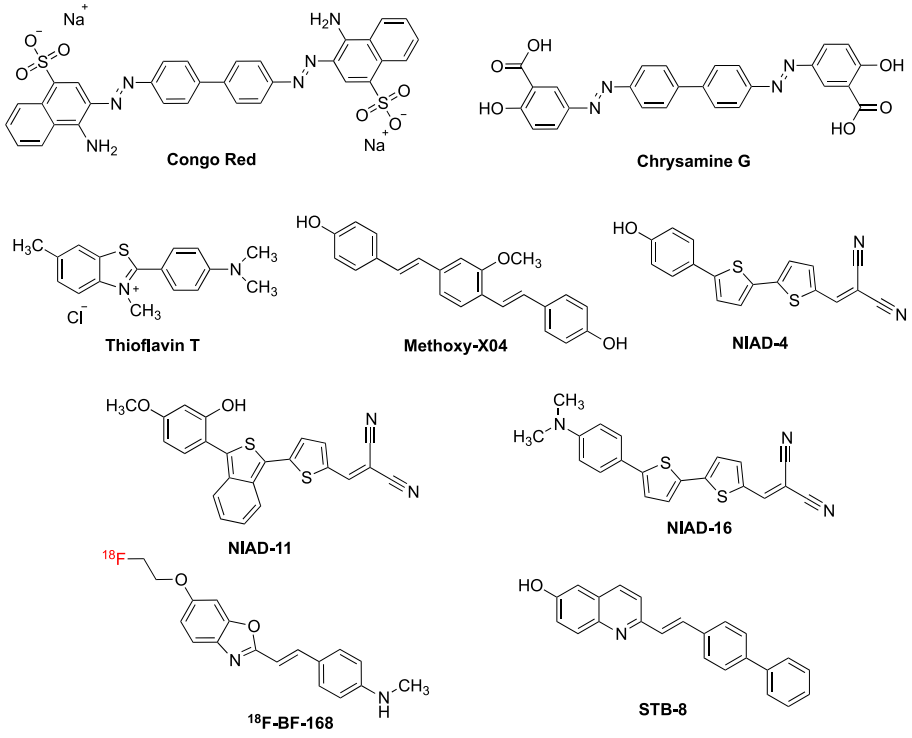

Fig. 6. Early theranostic agents against AD that target Aβ

compound-B (PiB), described in Section 3 due to its widespread use as a robust diagnostic tool in research. The process leading to PiB is depicted in Fig. 5.

Chrysamine G, X-34 and BSB (Fig. 6) are Congo red derivatives that bind to β-amyloid [72]. Another Congo red derivative, Methoxy-X04, works as a fluorescent probe marking amyloid deposits while exhibiting relatively high lipophilic character and ability to cross membranes [77]. Based on both Thioflavin T and in Congo Red, NIAD-4 was the first probe for amyloid staining that was detected for its fluorescence in the NIR, opening a new path into optical imaging. This compound was found to bind to Aβ with high affinity and specificity and marked the aggregates with high spatial resolution [78]. NIAD-4 crosses BBB, binds correctly to amyloid aggregates and has a good brain uptake. NIAD-11 and NIAD-16 present better spectral properties, with an emission maximum over 690 nm [79]. BF-168 is a thioflavin T analogue inspired in stilbene. ^{18}F–BF-168 labels amyloid deposits with little nonspecific binding and is a promising agent for the diagnosis of AD [80]. STB-8, another stilbene-like analogue of Thioflavin T, is also a reliable amyloid tracer with good BBB permeability [81].

There are many more amyloid tracers showing potential as diagnostic tools for AD that have not been designed or evaluated as therapeutic agents [82,83]. None of these compounds have made their way to clinical practice because of their low affinity, specificity or sensitivity, inability to cross BBB or significant toxicity. Thus, not many compounds marking Aβ have proved to block the aggregation of amyloid. It is true that most of them were not designed with this dual diagnostic-therapeutic objective in mind. Nevertheless, some scaffolds bear promising theranostic properties, such as Congo red and chrysamine G.

5.3. Cyanines

The research group led by Wong has made crucial contributions to the search and discovery of new theranostic compounds against AD. These probes have in common their ability to target amyloid and their optical imaging properties (NIR fluorescent imaging), in some cases added to magnetic resonance imaging in the case of hybrid small molecule-nanoparticle theranostics.

5.3.1. Carbazole cyanines

The first achievement of the Wong group in this area was the disclosure of SLOH, a candidate selected from a family of carbazole-based cyanines [84] (Fig. 7). This compound is fluorescent with an excitation maximum at λ_{ex} = 462 nm and an emission maximum at λ_{em} = 677 nm in phosphate buffer, and a low fluorescence quantum yield. SLOH binds to amyloid peptides, fibrils and plaques and, upon binding, experiences a strong fluorescence enhancement and a blue shift in its emission maximum to λ_{em} = 636 nm. This feature made SLOH suitable for optical imaging of Aβ, as confirmed by *in vitro* and *ex vivo* studies. Its potential therapeutic effect derives from its ability to inhibit Aβ aggregation and fibrillogenesis, as shown by *in vitro* tests. An MTT assay with neuroblastoma SH-SY5Y neuronal cells revealed that SLOH had a good safety, and *in vivo* mice studies showed its ability to cross BBB. A subsequent study assessed the therapeutic potential of SLOH in transgenic AD mice [85]. This *in vivo* evaluation had a promising outcome since SLOH reduced Aβ deposition and tau levels and hyperphosphorylation through the modulation of AKT and the promotion of protein phosphatase 2A activity, achieving a substantial improvement in the cognitive ability of treated transgenic mice. This study also reached the conclusion that SLOH attenuates synaptic deficit through the regulation of the signalling pathway Ca^{2+}/CaMKII/CREB, as observed in both *in vitro* and *in vivo* tests. In another study, SLOH was conjugated with Gadolinium Gd^{3+}-based nanoparticles, furnishing a probe that showed *in vivo* and *ex vivo* NIR imaging ability with high sensitivity and selectivity for Aβ oligomers and *in vivo* MRI with good spatial resolution, with *in vitro* potential therapeutic activities against amyloid aggregation and its toxic effects [86]. Thus, SLOH represents a good starting point for its theranostic potential against AD.

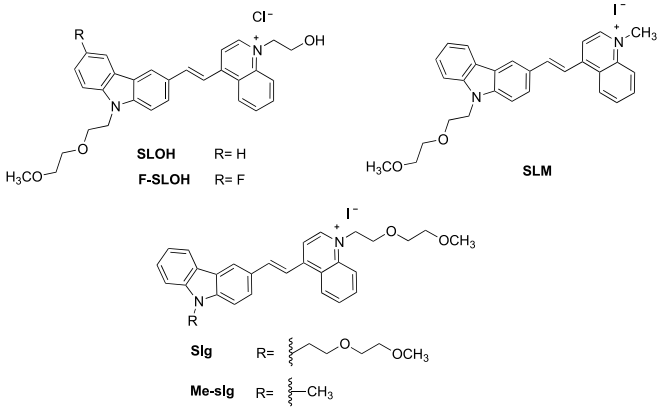

Fig. 7. Structures of carbazole-derived cyanine theranostic agents against AD.

A fluoro derivative of SLOH (F-SLOH) has exhibited a stronger binding selectivity when compared to SLOH, due to the combination of strong π-π stacking and intermolecular non-standard CH···O and CH···F hydrogen bonds. Interestingly, the interaction and fluorescence enhancement of F-SLOH was stronger with oligomers than fibrils. As a drawback, F-SLOH is only weakly fluorescent, with an excitation maximum at λ_{ex} = 470 nm and an emission maximum at λ_{em} = 643 nm in phosphate buffer, and a blue-shifted emission and fluorescence enhancement upon amyloid binding [87]. This compound is an efficient inhibitor of Aβ aggregation *in vitro*, as shown by circular dichroism spectroscopy and thioflavin T fluorescence assays for $A\beta_{40}$, and gel electrophoresis experiments for $A\beta_{42}$. More recent *in vivo* studies on transgenic mouse models revealed that F-SLOH inhibits Aβ aggregation, reduces the levels of amyloid monomers, oligomers and plaques, tau aggregates and APP and relieves synaptic deficits, synaptic memory function and cognitive impairment in AD mouse models, proving its promising *in vivo* therapeutic potential against AD [88]. Mechanistic studies showed an interesting ability of this compound to cleave a C-terminal fragment of APP and tau PHF through the activation of transcription factor EB (TFEB) and proved that it is also a regulator of autophagy and the autophagy lysosomal pathway. Interestingly, it was shown that brain clearance of F-SLOH is significantly faster in healthy mice than in transgenic AD mice, consistent with its binding and retention in AD brains. MTT assays on SH-SY5Y cells proved F-SLOH to be non-cytotoxic, and studies on primary hippocampus cells showed neuroprotective effect against Aβ-induced toxicity.

SLM was the first compound in the family to show promising diagnostic and therapeutic profiles in *in vivo* experiments. It is a fluorescent carbazole-based cyanine derivative with an excitation maximum at λ_{ex} = 455 nm and an emission maximum at λ_{em} = 677 nm in phosphate buffer, which undergoes a blue shift upon amyloid binding to an emission maximum at λ_{em} = 625 nm [84,89]. It has a poor fluorescence quantum yield, which represents a considerable drawback for its use as a theranostic. SLM binds strongly and specifically to Aβ monomers, oligomers and fibrils and, as the previously described compounds, it shows a strong fluorescence enhancement upon amyloid binding, which allowed the detection and imaging of Aβ species in a transgenic mouse model *in vivo* study. SLM behaved as a neuroprotective agent against neurotoxicity caused by $A\beta_{42}$ on primary hippocampal cells and reduced oxidative stress due to reactive oxygen species (ROS*) in vitro*. This compound was the first of these cyanine derivatives to undergo therapeutic activity tests *in vivo*, and thus its assessment against cognitive impairment was in transgenic AD model mice by the Morris water maze tests revealed that, after a 45-day SLM treatment, mice exhibited a significantly shorter latency to escape as compared to the control transgenic AD mice. The levels of Aβ and tau in the brains of these SLM-treated transgenic mice

were lower than in control mice, as well as GSK3β activity. Autophagy, whose dysfunction is linked to AD pathogenesis, was found to be modulated by SLM, helping to reduce Aβ and tau levels. SLM also displayed oligomerization inhibition activity in *in vitro* assays. Cytotoxicity in SH-SY5Y cells was found to be low by the MTT assay. Finally, *in vivo* and *ex vivo* BBB permeability results, as well as further pharmacokinetic studies, were satisfactory [90].

In continuation of these research efforts, Slg and Me-slg, two new carbazole-based cyanine fluorophores, were synthetised and evaluated in comparison to SLM [91], allowing the identification of Me-slg as the most promising candidate. This is a specially interesting molecule in this series due to its nanoscopic fluorescence imaging capability, allowing to image Aβ with a better spatial resolution. This feature is key for studying the toxicity of the different Aβ species, as conventional fluorescence microscopy lacked enough spatial resolution to do so. *In vitro* tests revealed that Me-slg is valid for real-time nanoscopic imaging of Aβ aggregates. *In vitro* tests on PC12 cells showed that the most toxic Aβ species were aggregates sized under the optical diffraction limit. This information about the morphology of amyloid aggregates mainly causing neurotoxicity was obtained thanks to the improved spatial resolution in nanoscopic images. Me-slg has an excitation maximum at λ_{ex} = 465 nm and an emission maximum at λ_{em} = 682 nm in phosphate buffer (pH 7.4). *In vitro* assays showed that inhibitor:protein ratios as low as 0.2 are sufficient for Me-slg to display a strong inhibitory effect on $A\beta_{40}$ fibrillization. This is mediated by a reduction in β-sheet folding processes, as observed through circular dichroism spectroscopy and in-silico modelling predictions. Me-slg also displayed neuroprotective effect and good biocompatibility in MTT assays on PC12 cell tests. Unfortunately, no *in vivo* studies are available for this compound to date.

5.3.2. Phenylamine-based cyanines

DMA-SLOH, DBA-SLOH and DPA-SLM (Fig. 8) were synthetised in the pursue of improved performance regarding amyloid affinity, inhibition potency, NIR-shifted emission and BBB permeability [92]. Among them, the one which showed the best diagnostic and therapeutic activities was DBA-SLOH. The introduction of lipophilic alkyl chains increases both the biocompatibility and the BBB-crossing ability. It is fluorescent with an excitation maximum at λ_{ex} = 550 nm and an emission maximum at λ_{em} = 672 nm in PBS, but a low fluorescence quantum yield. DBA-SLOH binds to amyloid species with high affinity and, upon binding, its fluorescence is enhanced and an approximately 20 nm blue shift in the emission maximum is observed. The ability of the compound to track amyloid species was confirmed in *in vitro* and *in vivo* mouse-model studies, representing a step forward from the starting point of SLOH. DBA-SLOH binds to monomers and aggregates and, in spite of its weak affinity to monomers, it prevents them from self-aggregating and forming toxic oligomers in *in vitro* experiments, an observation that reveals this compound as an interesting candidate for therapy. The compound was not found to be significantly cytotoxic in a MTT assay with neuroblastoma SH-SY5Y neuronal cells. In summary, DBA-SLOH is an interesting analogue of SLOH with improved biocompatibility and endowed with a theranostic profile.

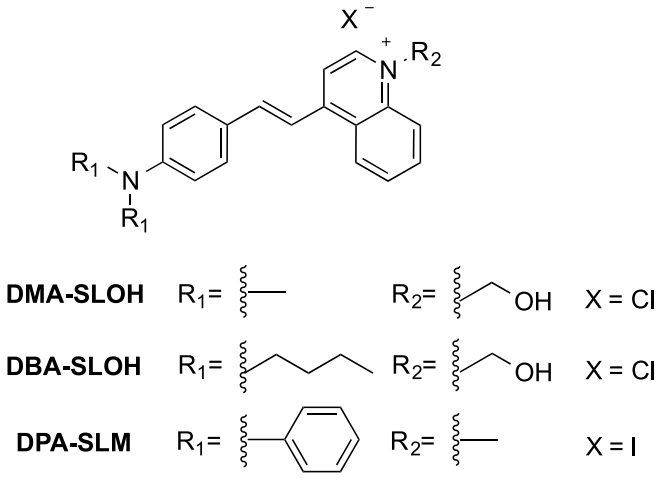

Fig. 8. Structures of phenylamine-derived cyanine theranostic agents against AD.

5.3.3. Naphthylamine-based cyanines

The replacement of carbazole by a 6-dibutylamino-2-naphthyl moiety expanded the chemical diversity of the cyanine AD theranostic probes and led to DBAN-SLOH, DBAN-SLM and DBAN-OSLM [93] (Fig. 9). Among them, the most promising one was DBAN-SLM, which binds with higher affinity to amyloid monomers and oligomers than to fibrils, as shown by the fluorescence enhancement observations. This selectivity towards monomers and oligomers is interesting due to their higher influence on AD pathology compared to fibrils. *In vivo* experiments with AD mouse models confirmed the targeting of DBAN-SLM towards Aβ without further specification of the species of amyloid. The fluorescent emission of the compound exhibits an excitation maximum at λ_{ex} = 486 nm and an emission maximum at λ_{em} = 615 nm in phosphate buffer, with very low fluorescence quantum yields. In contrast with the hypsochromic effect observed in carbazole- and phenylamine-cyanines, there is a bathochromic shift in the emission maximum upon amyloid binding, to wavelengths between 666 and 680 nm. This was further confirmed in *ex vivo* studies to be λ_{em} = 680 nm upon amyloid binding. DBAN-SLM exerted Aβ anti-aggregation activity *in vitro*, measured through a thioflavin T fluorescence assay. Regarding their neuroprotective effect, SH-SY5Y cell viability was compromised after incubation with amyloid species, but DBAN-SLM significantly reduced this toxic effect. Similarly, SH-SY5Y cells ROS production upon amyloid incubation was limited by the effect of DBAN-SLM. Cytotoxicity was found low in MTT assay on SH-SY5Y cells. These naphthylamine-derived cyanines are considerably less toxic than their phenylamine-based counterparts. DBAN-SLM BBB permeation was unequivocally observed *in vivo* using mice models, in contrast to DBAN-SLOH and DBAN-OSLM, with non-existent or low BBB permeability, respectively. In addition, DBAN-SLM was retained for longer times and showed stronger fluorescence signal in the brain of AD mouse models compared to control mice.

5.3.4. Miscellaneous cyanines

The Wong research group also developed hybrid small molecule-nanoparticle theranostics for AD. One of them was generated by the combination of the acid-functionalized cyanine sensor SLCOOH with superparamagnetic iron oxide nanoparticles [94] (Fig. 10). It was proved to be an effective NIR imaging and magnetic resonance imaging contrast agent for the imaging of Aβ species *in vivo*, with a good toxicity profile and neuroprotective effect against amyloid-induced toxicity) (see .

Another successful study in theranostics is represented by the conjugation of carbazole-based cyanine tracers with Gd(DOTA) that led to compounds **1** (Fig. 11), with promising properties as theranostic agents against AD [95]. Moreover, these molecules may be interesting because of their dual diagnostic nature encompassing NIR and MRI imaging, and may represent a solution to overcome low fluorescence quantum yields observed in cyanine-based small-molecule candidates. Other structurally-related compounds developed by the Wong research group showed *in vivo* therapeutic effect against AD, but their diagnostic potential was not evaluated [96].

SIM is a indolium-based turn-on fluorophore suitable for the quantification of trace amounts of amyloid peptide and tau protein and its hyperphosphorylated form in CSF, saliva, and urine, after labelling the corresponding antibodies directed towards these biomarkers [97]. Additional cyanines employed in investigations related to theranostics in AD include N744, a dye that was shown to block tau fibrillization but

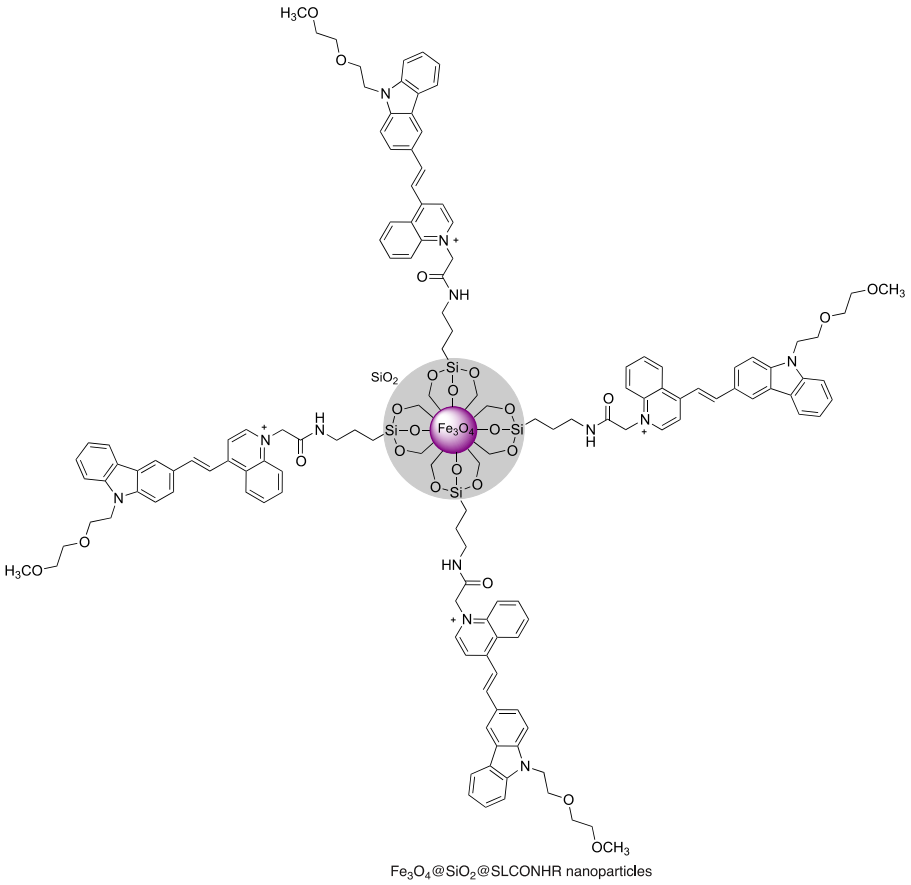

Fig. 10. Theranostic nanoparticles based on a cyanine dye.

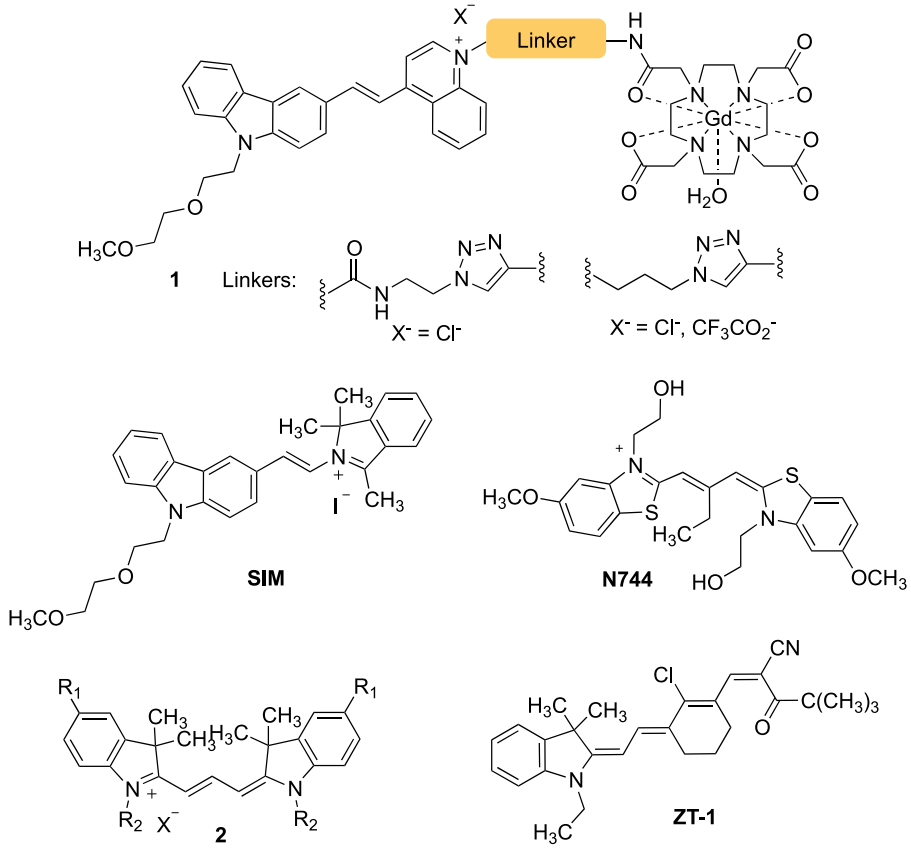

Fig. 11. Miscellaneous cyanine dyes.

was not further studied [98,99]. A more recent achievement was the disclosure of fluorescent trimethine cyanine dyes **2** as sensitive and biocompatible tracers for optical imaging of tau fibrils in human AD brain and olfactory epithelium, although lacking therapeutic activity studies [100]. Another example is ZT-1, a hemicyanine derivative capable of detecting amyloid aggregates with suitable properties as a diagnostic tool, but lacking further studied applications for therapeutic purposes [101].

5.4. Curcumin-based theranostic compounds

The research area was initiated by Ran and Moore with the disclosure of curcumin analogues as potential theranostic candidates against AD and has given birth in recent years to a growing number of different molecules with diverse mechanisms for its detection and imaging, mostly through NIR fluorescent imaging [102].

5.4.1. CRANAD-2

Curcumin has long been considered as a good starting point for the development of diagnostic and therapeutic tools against AD since it can bind and stain Aβ and prevent plaque deposition; on the negative side, curcumin has a fast metabolism and a short emission wavelength and shows limited BBB crossing [103,104]. To overcome these drawbacks, Ran et al. designed a series of curcumin derivatives bearing a difluoroboronate moiety. CRANAD-2 (Fig. 12) was found to be the most interesting one, showing good fluorescent properties with an excitation maximum at $\lambda_{ex} = 640$ nm and an emission maximum at $\lambda_{em} = 805$ nm in PBS, displaying a large Stokes shift, and an improved quantum yield compared to that of curcumin [105]. In spite of these advantages, CRANAD-2 has a low fluorescent quantum yield. *In vitro* tests revealed that this probe experienced a 70-fold increase of its fluorescent intensity upon binding to Aβ aggregates, which can be described as a turn-on phenomenon, as well as a 90 nm blue shift of the emission maximum. The suitability of CRANAD-2 to detect Aβ was confirmed, first, by *in vitro*

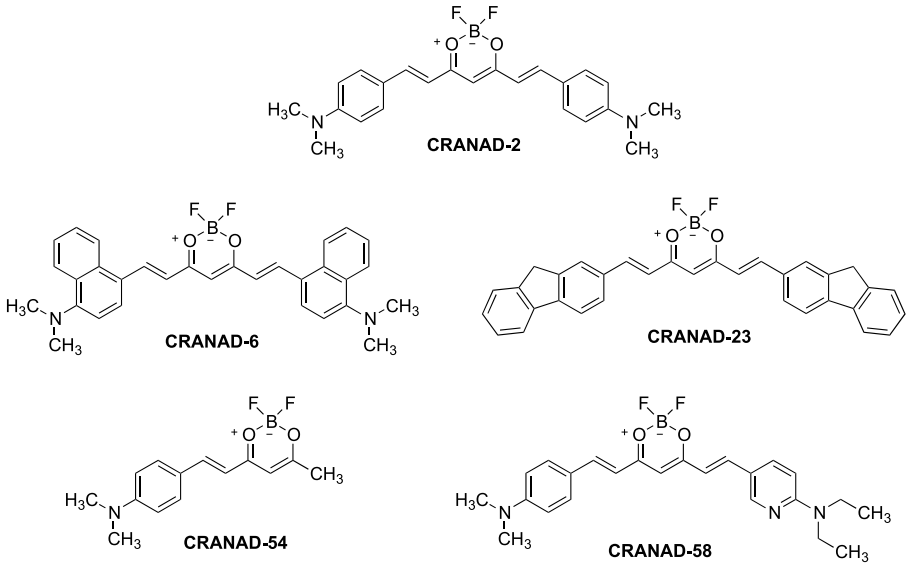

Fig. 12. Curcumin-derived theranostic agents: CRANAD compounds.

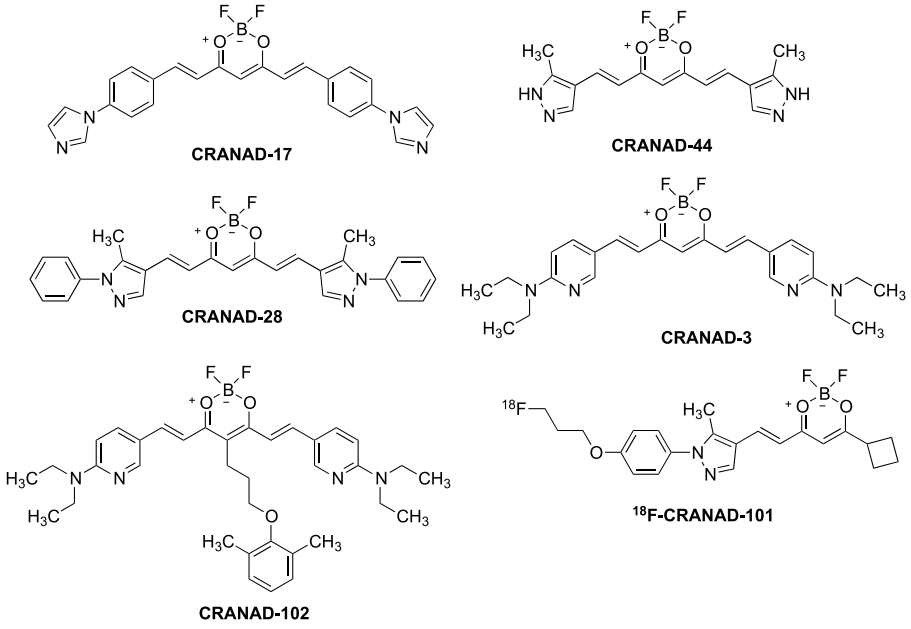

Fig. 13. CRANAD compounds (continued).

tests and later with *in vivo* AD mouse model fluorescence imaging studies and *ex vivo* with histological assays. Its BBB permeability was assessed *in vivo* with wild-type mice model, with a positive result. In subsequent studies it was unveiled that CRANAD-2 cannot detect soluble Aβ species [106].

5.4.2. CRANAD-6, CRANAD-23, CRANAD-54 and CRANAD-58

Efforts to overcome the inability of CRANAD-2 to detect soluble amyloid species led to the design of CRANAD-6 and CRANAD-23 [107]. These compounds have extended conjugated rings compared to CRANAD-2, which was expected to have a positive influence on binding owing to retention in a hydrophobic site. However, none of these compounds were able to bind to amyloid, which was interpreted to mean that the binding of CRANAD-2 to amyloid fibrils is sensitive to steric hindrance, and a new binding site union was hypothesised. To obtain more information about this hypothesis, CRANAD-54, one half of the symmetric CRANAD-2, was synthetised and tested, providing new and valuable information about binding [107]. Additionally, CRANAD-58, having one half of the molecule with a predominantly hydrophobic behaviour and the other half displaying a more hydrophilic character thanks to a pyridyl moiety, was also designed [107]. This compound showed fluorescence changes upon binding to both soluble and insoluble amyloid species *in vitro* and was able to distinguish between AD transgenic mice and wild-type mice at an age of 4-months, when no amyloid plaques are observed yet, thus indicating its interaction with soluble forms. It can thus be concluded that *in vitro* and *in vivo* studies confirmed CRANAD-58 binding and marking all forms of Aβ.

5.4.3. CRANAD-17, CRANAD-44 and CRANAD-28

Copper can coordinate to two imidazole moieties at histidine residues of Aβ, inducing cross-linking of amyloid. CRANAD-17, bearing two imidazole moieties (Fig. 13), was designed to interfere with this mechanism and alleviate cross-linking [107]. *In vitro* tests, SDS-PAGE gel and Western blot studies disclosed that CRANAD-17 can inhibit $A\beta_{42}$ copper-induced cross-linking, revealing a mechanism to introduce therapeutic activity in these scaffolds.

The replacement of the phenyl rings in CRANAD-2 by electron-withdrawing pyrazoles was expected to reduce electron delocalisation and increase the quantum yield. Also, pyrazole can coordinate with copper, potentially inhibiting cross-linking like CRANAD-17. CRANAD-28 [108] showed an excitation maximum at λ_{ex} = 498 nm and an emission maximum at λ_{em} = 578 nm in PBS (pH 7.4), and displayed a high fluorescence quantum yield, as expected. To confirm that the N-1 substitution of pyrazole in CRANAD-28 reduces the non-radiative emission decay and increases the quantum yield, CRANAD-44 was synthesised, showing a lower quantum yield and confirming the hypothesis [108]. *In vitro* assessment of both compounds for their binding to amyloid was performed. While CRANAD-28 showed an unexpected decrease of fluorescent intensity upon mixing with soluble and insoluble forms of Aβ, CRANAD-44 did not show significant changes with soluble amyloid. *In vitro* assays using AD-mouse-model brain slices revealed that CRANAD-28 labels amyloid plaques properly, while CRANAD-44 does not. *In vivo* studies on transgenic AD mouse model with two-photon imaging confirmed the ability of CRANAD-28 to cross BBB and to label amyloid plaques and cerebral amyloid angiopathies as well. This is the proof of the potential diagnostic activity of CRANAD-28. In the search for a combined therapeutic activity, CRANAD-28 was tested and confirmed to inhibit not only copper-induced but also natural-occurring cross-linking *in vitro*, unlike CRANAD-44 for both phenomena. Therefore, CRANAD-28 is the first CRANAD curcumin analogue displaying both diagnostic and therapeutic activity. In subsequent studies, CRANAD-28 proved to be a promising tool for the visualization and tracking of amyloid plaque development *in vivo* and displayed different spectral characteristics when labelling amyloid at the periphery of plaques with longer emission wavelengths than that of the core region [109].

5.4.4. CRANAD-3 and CRANAD-102

CRANAD-3 was involved in the first example of the use of a NIR fluorescence imaging probe to monitor changes in the load of amyloid in an AD mouse model during therapy with a known beta-amyloid cleaving enzyme-1 (BACE-1) inhibitor, LY2811376, and also with CRANAD-17. CRANAD-3 was found to successfully monitor AD therapy with these treatments [110], meeting for the first time the need for a versatile, sensitive, low-cost, easy to obtain, use and data process diagnostic tool, especially for AD preclinical research. PET probes are useful but lack these characteristics, their synthesis is complex and needs to be carried out right before use.

CRANAD-3 was designed by modification of the two phenyl rings of CRANAD-2, which are related to its inability to bind to soluble amyloid species and were replaced by two pyridyls, providing the molecule with a more hydrophilic nature. The fluorescent properties of CRANAD-3 include an excitation maximum at λ_{max} = 600–610 nm and an emission maximum at λ_{max} = 730 nm in PBS (pH 7.4). It binds strongly to Aβ monomers, dimers and oligomers, and undergoes a wavelength shift upon binding. *In vitro* tests showed CRANAD-3 to be selective towards amyloid and able to bind to soluble and insoluble Aβ, particularly to the core fragment KLVFF. The compound also labelled amyloid in transgenic AD mice which could be assessed *in vivo* through two-photon microscopy and NIR fluorescence imaging, and on *ex vivo* histology. Both *in vivo* -AD mouse model- and *ex vivo* studies confirmed BBB permeability of the molecule. In summary, CRANAD-3 presents a good diagnostic ability against AD.

CRANAD-102 is a derivative of CRANAD-3 having a phenoxy-alkyl chain at the central carbon of the dioxaborine system. Stereohindrance tuning by this structural modification resulted in a respectable selectivity for soluble over insoluble Aβ (68-fold), coupled to a strong affinity. As a consequence, CRANAD-102 was employed to dynamically monitor the concentration of soluble Aβ in both 5-month-old and 12-month-old AD transgenic [111].

5.4.5. CRANAD-101

This compound was the first PET probe based on a curcumin CRANAD-like scaffold and was designed to overcome the limitations of ^{18}F-labelled first generation probes such as florbetaben, florbetapir, and flutemetamol. Based on the information obtained from CRANAD-54, the synthesis of a PET derivative, ^{18}F-CRANAD-54, was attempted, but met with failure due to low yields, difficult purification and unfavourable synthetic conditions for PET tracers. For this reason, and based on CRANAD-28, a half-curcuminoid derivative bearing a cyclobutyl moiety on the reactive end of the diketone was synthesised, yielding CRANAD-101, which finally underwent ^{18}F-radiolabelling [112]. *In vitro* tests revealed that non-radiolabelled F-CRANAD-101 binds to both soluble and insoluble amyloid forms, but *ex vivo* studies could only confirm binding to insoluble species due to the limits of conventional fluorescence microscopy. *In vivo* assays proved that F-CRANAD-101 can label amyloid plaques. ^{18}F-CRANAD-101 underwent PET imaging evaluation *in vivo* with a transgenic AD mouse model with positive results for amyloid labelling and BBB permeation. Further *in vivo* PET imaging was performed with a 5-month-old transgenic AD mouse model, in which soluble Aβ are the main species before insoluble fibrils and plaques form, showing significant retention compared to wild-type mice.

5.4.6. Miscellaneous CRANAD and related compounds

Recently, Fang et al. designed a new set of CRANAD-like derivatives aimed at improving the relatively short emission wavelength of CRANAD-58 [113]. Among these molecules, compound **3** (Fig. 14) stood out as the most promising one. It showed high sensitivity and selectivity towards Aβ and displayed a higher quantum yield and longer fluorescent emission wavelengths upon binding to amyloid than those of CRANAD-58 ($\lambda_{em\ max}$ = 688–697 nm), also showing a "turn-on" behaviour upon binding with a remarkable increase in its fluorescent emission intensity. Compound **3** was found to cross BBB and properly

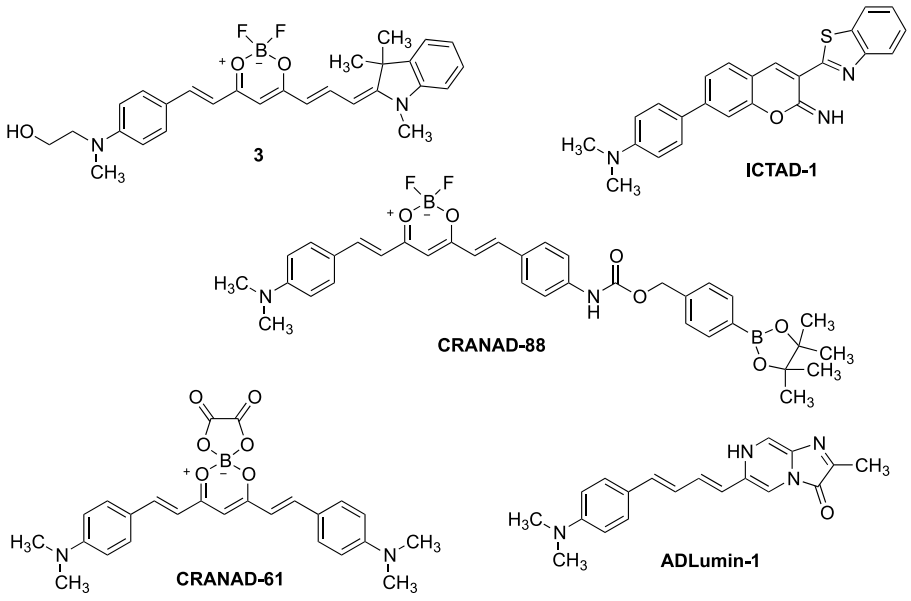

Fig. 14. CRANAD compounds (continued).

label Aβ *in vivo*. In *in vivo* experiments, tests using 6-month-old and 10-month-old AD mouse models (representative of mainly soluble and insoluble amyloid species, respectively) showed that compound **3** was able to differentiate them from age-matched wild type mice, confirming the potential of this candidate to label both soluble and insoluble forms of amyloid. *In vitro* assays revealed that compound **3** has a higher inhibitory activity against amyloid aggregation than CRANAD-58, making it a potential theranostic candidate against AD.

Other efforts from the Ran group, so far exclusively related to diagnostic purposes, include the development of an iminocoumarin–thiazole probe, ICTAD-1, for the differentiation of $A\beta_{40}$ and $A\beta_{42}$ fibrils [114], the disclosure of CRANAD-88, a probe capable of cascade amplifying NIR fluorescence signals upon interacting with H_2O_2 in AD brains [115], and the application of several curcumin analogues to the detection of amyloid species in the retina of AD animal models as an alternative for the diagnosis of AD [116]. Additional important milestones are the design of a ROS-sensitive probe, CRANAD-61, which underwent wavelength shifting upon reaction with ROS [117] and, more recently, the development of a turn-on chemiluminescence probe, ADLumin-1 [118]. All of these compounds can provide innovative approaches to diagnose and monitor AD and its pathogenic mechanisms, and can therefore be the starting point for key discoveries and the development of novel diagnostic and therapeutic tools against AD.

5.5. Phenothiazine derivatives

Phenothiazines have been proposed as useful scaffolds for the development of theranostic agents against AD. Thus, in 2017, Dao et al. disclosed a series of phenothiazine-based compounds with promising properties as theranostic agents against AD (Fig. 15) [119]. Compound **4**, in particular, showed the highest affinity to Aβ aggregates. *In vitro*, it was able to bind to and label amyloid plaques in brain slices and retina tissue of transgenic AD mice. Developed as a NIR fluorescent probe, it has an excitation maximum at $\lambda_{ex} = 500$ nm and an emission maximum at $\lambda_{em} = 680$ nm in PBS (pH 7.4). The emission maximum shifts to 670 nm and there is a fluorescent emission intensity enhancement upon binding to

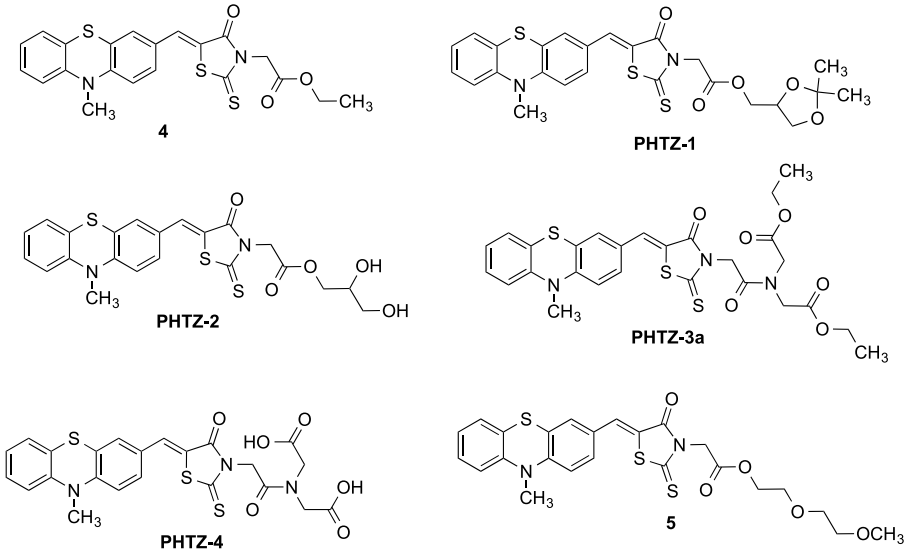

Fig. 15. Phenothiazine-based theranostic agents against AD.

$A\beta_{42}$ amyloid aggregates, but not in response to $A\beta_{42}$ monomers. The cytotoxicity was assessed in the MTT assay with SH-SY5Y neuronal cells, which showed a good safety of compound **4**. The compound exhibited a strong amyloid aggregation inhibition *in vitro* and was found to promote the disassembly of amyloid fibrils *in vitro*, showing an interesting double therapeutic profile of anti-aggregation and disintegration activities. Despite these promising properties, the poor water solubility exhibited by compound **4** has prevented it from undergoing further development as a NIR fluorescent probe *in vivo* [120].

In order improve aqueous solubility of these scaffolds and also to achieve metal chelating capability, an interesting mechanism to tackle AD also present in CRANAD-17 and CRANAD-28, new phenothiazine derivatives (compounds PHTZ) were synthetised and tested [121] and they exhibited fluorescent emission with their emission maxima over 640 nm in PBS, except for PHTZ-4, making them interesting for NIR fluorescent imaging. They showed good binding affinity towards Aβ aggregates, and upon binding to them, the emission maxima of PHTZ-1, PHTZ-2 and PHTZ-3a experienced a blue shift to 615 nm and a fluorescent intensity enhancement. In particular, PHTZ-1 had the highest binding affinity for amyloid aggregates and a significant increase in fluorescent emission upon binding. For this reason, PHTZ-1 was chosen for further assays, which proved its ability to detect and label Aβ plaques, both *in vitro* with AD-mouse brain slices and *in vivo* in AD mouse models. This molecule also inhibited Aβ aggregation in *in vitro* assays on SH-SY5Y neuronal cells with a more potent activity than that of previous phenothiazine-based compounds. *In vitro*, all of these new PTHZs were found to provide a neuroprotective effect against amyloid-induced toxicity and a reduction of ROS species on SH-SY5Y neuronal cells studies. These compounds also displayed metal-chelating activity as tested for Cu^{2+} ions in UV/Vis titration. Cytotoxicity was assessed in the MTT assay using SH-SY5Y cells, showing a good profile for PHTZs. Finally, computational predictions demonstrated a better water solubility for these PHTZs over previously studied phenothiazine-based compounds.

Another approach to overcome the water-solubility issues associated to the first generation of phenothiazine-based involved introducing polyether water solubilizing groups [120]. Compound **5**, the most promising of this series, is a fluorescent molecule with an excitation maximum at $\lambda_{ex} = 482$ nm and an emission maximum at $\lambda_{em} = 670$ nm in PBS, the latter undergoing blue-shifting to 610 nm and experiencing a considerable increase in the fluorescent emission intensity upon binding to Aβ aggregates in PBS. Viability experiments on SH-SY5Y cells showed a low toxicity for compound **5**. BBB permeation and amyloid plaque detection and labelling was efficient in *in vivo* experiments with AD mice, and its binding to Aβ plaque was proved *ex vivo* on brain slices of previously intravenously injected AD mice. This molecule displayed amyloid aggregation inhibition in *in vitro* assays, as well as a neuroprotective effect against amyloid-induced toxicity in SH-SY5Y-cell *in vitro* studies.

5.6. Styrylquinolines

Styrylquinolines have also emerged as promising scaffolds for the search of theranostic agents in AD. We have shown compound **6** (Fig. 16) to have native fluorescence, with an excitation maximum at $\lambda_{ex} = 370$ nm and an emission maximum at $\lambda_{em} = 557$ nm in PBS (pH 7.4). *In vitro* studies found this compound able to bind to Aβ with high affinity, to stain it and to inhibit its aggregation. Upon binding to Aβ, the emission maximum shifts to 490 nm. The toxicity profile of the compound was good, as shown by *in vitro* tests [82]. Finally, the PAMPA test predicted that this compound is able to cross BBB. On the basis of these promising features, a new family of styrylquinoline-based compounds (compounds **7**) was designed, having a push-pull structure where a malononitrile moiety is the electron-withdrawing group [122]. These molecules exhibit fluorescent emission shifted towards the NIR region, with emission maxima above 600 nm in dioxane, with a significant enhancement of their fluorescent intensity in non-polar solvents as well as upon binding to amyloid fibrils. Some of the compounds were proved to bind and label Aβ *ex vivo*, and all the compounds were able to inhibit tau aggregation *in vitro* using an hexapeptide AcPHF6 model. They were also shown to exert neuroprotective activity in several cellular models of neurotoxicity related to Alzheimer's disease. The toxicity of the compounds was tested using the MTT assay, finding no major toxicity issues. These results confirm the styrylquinoline scaffold as an interesting structure for the development of theranostic agents against AD.

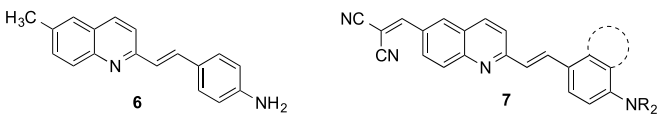

Fig. 16. Styrylquinoline-based theranostic agents against AD.

5.7. Crown ethers and their aza analogues

Some crown ethers and their aza equivalents have demonstrated potential therapeutic and diagnostic activities against AD. The structures of the most interesting ones are shown in Fig. 17.

5.7.1. PiB-C

PiB-C, developed by Ran and Moore, results from the combination of the above-mentioned Pittsburgh compound-B (PiB) with 12-crown-4 ether [123]. Crown ethers are known to form stable hydrogen bonds with protonated amines, allowing an efficient interaction with basic residues of Aβ and the subsequent cleavage of salt bridges, key for protein misfolding, and therefore attenuating amyloid aggregation. For compound design, 12-crown-4 ether was chosen due to its low molecular weight and its lack of interference in the homeostasis of the physiologically important ions Na^+ and K^+. It was found to modify the zeta potential and thus the surface charges of Aβ and mitigate amyloid aggregation *in vitro*. These properties of 12-crown-4 ether were targeted specifically towards Aβ by connecting it to PiB, yielding the PiB-C compound, which could also modify the zeta potential of the fibrils and inhibit amyloid aggregation *in vitro*. The fact that PiB-C displayed stronger inhibitory activity than PiB meant that the crown ether moiety contributes to the inhibitory effect. Neuroprotection assays on SH-SY5Y cells showed that 12-crown-4 ether itself and PiB-C reduced Aβ-induced toxicity, while PiB did not. Regarding its evaluation as a diagnostic tool, *in vitro* and *in vivo* studies demonstrated the ability of PiB-C to label amyloid plaques. BBB permeation was also tested and confirmed *in vivo*. PiB-C showed similar fluorescent properties to PiB and was detected with two-photon imaging. The short wavelength of the fluorescent emission maximum, found to be below 500 nm, represents a significant drawback for the application of PiB-C as a diagnostic tool through fluorescence imaging. This limitation notwithstanding, PiB-C represents a promising starting point for the development of theranostic candidates against AD.

5.7.2. TBT

TBT is a fluorescent derivative of thioflavin T and PiB containing a metal chelator group, which can be viewed as an analogue of PiB-C [124]. The compound is an aza-crown ether, 1,4,7,10-tetraazacyclododecane or cyclen, a structural analogue of a crown ether, but the strategy towards the treatment of AD differs in comparison to that of PiB-C. Metal ions like zinc, copper, iron and calcium can promote amyloid aggregation and toxicity, so metal chelators may represent an opportunity for the development of therapeutic alternatives against AD [125]. The PiB-like scaffold provides TBT with affinity towards Aβ, like in the case of PiB-C, but the aza-crown ether is aimed at behaving as a metal chelator group and reduce the metal-induced amyloid aggregation, instead of interfering with the formation of salt bridges needed for the interactions of misfolded proteins. These two different approaches for such similar structures may represent a wider opportunity for the

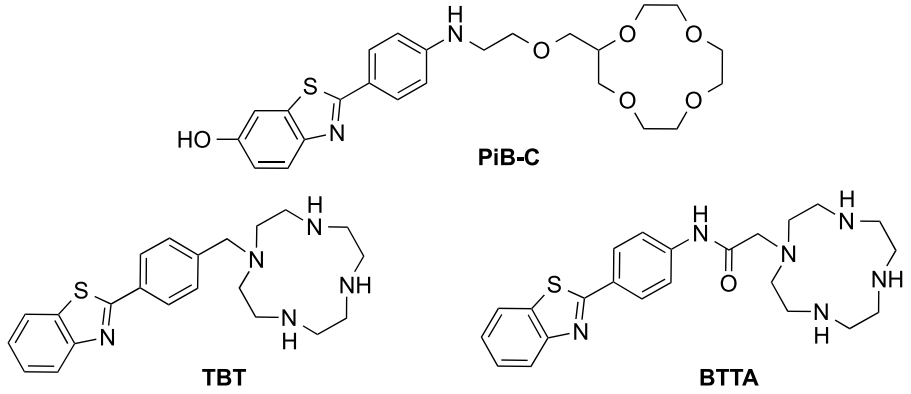

Fig. 17. Structures of crown ether and aza crown ether-based theranostic agents against AD.

achievement of therapeutical activity. TBT is fluorescent due to the PiB-based fragment and this fluorescence is modulated by the photoinduced electron transfer effect of the amino groups of the cyclen scaffold upon its coordination with metal ions. Through fluorescence titration, TBT was found to firmly bind to Zn^{2+} and Cu^{2+} through the cyclen moiety, with a high selectivity for Cu^{2+} when compared to other physiologically relevant ions (Na^{+}, K^{+}, Ca^{2+}, Fe^{2+}, Fe^{3+} and Al^{3+}, among others). To translate this interesting feature into a potential therapeutic application, the affinity of TBT towards Zn^{2+}-$A\beta_{40}$ aggregates was assessed and found to be high, and TBT was also shown to displace thioflavin T when binding to these associated metal-amyloid species, but not in the absence of metal ions. *In vitro*, TBT also displayed a significant disaggregation activity for Cu^{2+}/Zn^{2+}-induced $A\beta_{40}$ aggregates, stronger to that achieved by cyclen alone, which points to a synergistic effect resulting from the combination of the metal chelator moiety and the amyloid-targeting scaffold. This disaggregation activity could be tracked in PBS through an increase in the fluorescence intensity of TBT along the process because of the blockage of photoinduced electron transfer phenomena with Zn^{2+} [126]. The disassembly effect was not found for metal-free amyloid aggregation. The ability to disassemble metal-induced $A\beta_{40}$ aggregates was further evaluated in AD-mouse brain homogenates. TBT produced a significant increase in the amount of oligomeric amyloid species, thus providing a disaggregating activity. In this case, a decrease in the fluorescence intensity was observed, which was related to coordination with Cu^{2+} and its strong paramagnetic character, and could still be useful for the monitorization of the process [126]. TBT also relieved the neurotoxicity induced by metal-amyloid species in MTT assays using PC12 cells. In addition, TBT could cross BBB and be easily cleared from the brain *in vivo*. Further *in vivo* evaluation of the clinical translation of these effects could confirm the potential application of TBT as a theranostic agent against AD. However, the short wavelength of the emission maximum in response to metal ions, λ_{em} = 375 nm in buffer (20 mM Tris-HCl, 150 mM NaCl, 8‰ v/v DMSO, pH 7.4), represents an important drawback of this compound for fluorescent imaging.

5.7.3. BTTA

Another interesting PiB-derivative containing the aza-crown ether cyclen as a metal chelator, namely BTTA, was developed [127]. In this case, the structure is more similar to PiB-C than that of TBT, with the introduction of an amide group in the linker between the PiB-like scaffold and the cyclen moiety, which implies the conservation of the aliphatic nitrogen of PiB that was lost in the design of TBT. These modifications were prompted by the goal of increasing the fluorescence quantum yield and diminishing the photoinduced electron transfer effect of the amines of the cyclen scaffold, thus increasing the selectivity towards Cu^{2+} ions. Indeed, fluorescence titration experiments show that BTTA has a high sensitivity and binding affinity towards copper ions over other metal ions. In a similar way to TBT, BTTA has a higher binding affinity towards Cu^{2+}-associated amyloid species than to metal-free aggregates, displacing ThT from its binding to amyloid in the presence of Cu^{2+} in a competition assay. *In vitro* studies revealed that BTTA exhibits copper-associated amyloid aggregates disaggregation activity, releasing soluble amyloid species, an activity that was not found towards Cu^{2+}-free amyloid aggregates. In addition, BTTA provided a protective effect against Cu^{2+}-amyloid induced neurotoxicity, as revealed by MTT assay with PC12 cells. *In vitro*, BTTA was found to disassemble Cu^{2+}-amyloid aggregates and monitor its own disaggregating activity through a decrease in its fluorescence intensity, both in preformed amyloid aggregates assays and in brain homogenates of AD mouse models. These effects were not observed on Cu^{2+}-free amyloid aggregates. Further studies showed that BTTA was able to detect and label amyloid aggregates through fluorescence imaging *ex vivo*. Also, BTTA can cross BBB as proved with *in vivo* studies on mice. Further development of this probe is needed because its short fluorescence emission wavelength, with an excitation maximum at λ_{ex} = 318 nm and an emission maximum at λ_{em} = 386 nm in buffer (20 mM Tris-HCl, 150 mM NaCl, 8‰ v/v DMSO, pH 7.4), represents an important limitation for *in vivo* imaging.

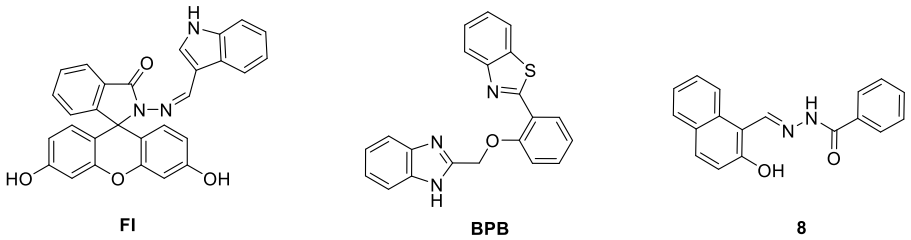

Fig. 18. Structures of miscellaneous theranostic agents against AD.

Table 1
Summary of the characteristics of potential theranostic agents against AD.

Family	Compound	Type of probe	Diagnostic activity	Therapeutic activity	Comments
Cyanines	**SLOH**	Fluorescent	*In vitro* and *ex vivo*	*In vitro* and *in vivo*	Low fluorescence quantum yield
	F-SLOH	Fluorescent	*In vitro* and *in vivo*	*In vitro* and *in vivo*	Low fluorescence quantum yield
	SLM	Fluorescent	*In vitro* and *in vivo*	*In vitro* and *in vivo*	Low fluorescence quantum yield
	DMA-SLOH, **DBA-SLOH** and DPA-SLM	Fluorescent	*In vitro* and *in vivo*	*In vitro*	Low fluorescence quantum yield
	Me-slg and Slg	Fluorescent	*In vitro* (nanoscopic resolution)	*In vitro*	Low fluorescence quantum yield. No *in vivo* studies
	DBAN-SLM, DBAN-SLOH and DBAN-OSLM	Fluorescent	*In vitro, ex vivo* and *in vivo* (selectivity towards monomers and oligomers)	*In vitro*	Low fluorescence quantum yield
Curcumin derivatives	**CRANAD-2**	Fluorescent	*In vitro, ex vivo* and *in vivo* (cannot detect soluble Aβ species)	–	Low fluorescence quantum yield
	CRANAD-6	Fluorescent	–	–	Does not bind to Aβ
	CRANAD-23	Fluorescent	–	–	Does not bind to Aβ
	CRANAD-54	Fluorescent	Provided important information about binding to Aβ (*in vitro*)	–	Short fluorescent emission wavelengths
	CRANAD-58	Fluorescent	*In vitro* and *in vivo*	–	–
	CRANAD-17	Fluorescent	–	*In vitro* (inhibition of $A\beta_{42}$ copper-induced cross-linking)	–
	CRANAD-44	Fluorescent	–	–	Does not bind to Aβ
	CRANAD-28	Fluorescent	*In vitro* and *in vivo*	*In vitro* (inhibition of copper-induced and also natural-occurring cross-linking of amyloid)	Unexpected decrease of fluorescent intensity upon binding to Aβ
	CRANAD-3	Fluorescent	*In vitro, ex vivo* and *in vivo* (useful for monitorization of amyloid levels during therapy *in vivo*)	–	–
	CRANAD-101	PET	*In vitro, ex vivo* and *in vivo*	–	–
	Compound 3	Fluorescent	*In vitro* and *in vivo*	*In vitro*	–
Phenothiazines	**Compound 4**	Fluorescent	*In vitro*	*In vitro*	Low water solubility
	PHTZ-1	Fluorescent	*In vitro* and *in vivo*	*In vitro*	–
	Compound 5	Fluorescent	*In vitro, ex vivo* and *in vivo*	*In vitro*	–
Family	Compound	Type of probe	Diagnostic activity	Therapeutic activity	Comments
Styrylquinolines	**Compound 6**	Fluorescent	*In vitro*	*In vitro*	Short fluorescent emission wavelength
	Compounds 7	Fluorescent	*Ex vivo*	*In vitro*	-
Crown ethers and aza crown ethers	**PiB-C**	Fluorescent	*In vitro* and *in vivo*	*In vitro* (modification of the zeta potential of the fibrils and inhibition of amyloid aggregation)	Short fluorescent emission wavelength
	TBT	Fluorescent	*In vitro*	*In vitro* (disaggregation activity for Cu^{2+}/Zn^{2+}-induced $A\beta_{40}$ aggregates)	Short fluorescent emission wavelength
	BTTA	Fluorescent	*In vitro* and *ex vivo*	*In vitro* (disaggregation activity for Cu^{2+}-amyloid aggregates and monitorization of this disaggregation)	Short fluorescent emission wavelength
Others	**FI**	Fluorescent	*In vitro*	*In vitro*	Short fluorescent emission wavelength
	BPB	Fluorescent	*In vitro* and *in vivo* (distinguishes among $A\beta_{40}$ and $A\beta_{42}$ *in vitro*, and detects amyloid oligomers in blood *in vivo*)	*In vitro*	Short fluorescent emission wavelength
	Compound 8	Fluorescent	*In vitro* (fluorescence emission activation upon combination with Al^{3+} ions)	*In vitro*	Short fluorescent emission wavelength

5.8. Miscellaneous theranostic agents

FI (Fig. 18) is an hydrazone derived from indole-3-carboxaldehyde and fluorescein with promising features as a theranostic candidate against AD [128]. From a therapeutic perspective, this molecule was able to chelate Cu^{2+} from preformed amyloid aggregates, as stated in studies where the decrease of the fluorescence of a tyrosine residue of Aβ due to binding to Cu^{2+} was used as a reference and a new emission peak at 518 nm upon excitation with 465 nm light was found, corresponding to the emission maxima of FI- Cu^{2+} complexes. This was explained as a consequence of the opening of the spirolactam ring by Cu^{2+} after some incubation time with Cu^{2+}-amyloid aggregates, thus providing a fluorescent turn-on effect *in vitro*. On the other hand, incubation with Cu^{2+}-free Aβ aggregates did not display this turn-on effect. In addition, FI showed higher affinity for copper ions than $A\beta_{40}$ and potential to chelate them from Aβ. Further experiments using real CSF, lysozyme Aβ aggregates and human astrocyte cells proved the ability of FI to chelate Cu^{2+} from amyloid aggregates and disassemble and prevent reaggregation of amyloid fibrils. This probe could even disaggregate Aβ without copper ions *via* noncovalent interactions with amyloid fibrils. Additional imaging techniques could determine the transformation of the β-sheet structure of Aβ aggregates into a random coil upon incubation with FI. MTT assay showed a good toxicity profile for FI, and BBB permeation was tested in an *in vitro* model of a monolayer of endothelial cells, which FI was able to cross. Further studies *in vivo* are required to fully understand the role of FI as a potential metal-chelator theranostic candidate for AD.

BPB is a hybrid structure resulting from the combination of two

Table 2
Summary of the optical features of potential theranostic agents against AD.

Family	Compound	Excitation wavelength	Emission wavelength	Fluorescence quantum yield in PBS	References
Cyanines	**SLOH**	462 nm (PBS)	677 nm (PBS)636 nm (with Aβ fibrils)	0.0033	[84–86]
	F-SLOH	470 nm (PBS)	643 nm (PBS)620–625 nm (with Aβ fibrils)	0.006	[87,88]
	SLM	455 nm (PBS)	677 nm (PBS)625 nm (with Aβ fibrils)	0.0014	[84,89,90]
	DMA-SLOH	520 nm (PBS)	664 nm (PBS)	0.007	[92]
	DBA-SLOH	550 nm (PBS)	672 nm (PBS) 650–655 nm (with Aβ fibrils)	0.006	[92]
	DPA-SLM	505 nm (PBS)	685 nm (PBS)	0.003	[92]
	Me-slg	465 nm (PBS)	682 nm (PBS)	~ 0.005	[91]
	Slg	467 nm (PBS)	674 nm (PBS)	–	[91]
	DBAN-SLM	486 nm (PBS)	615 nm (PBS) 666–680 nm (with Aβ monomers, oligomers and fibrils)	0.02	[93]
	DBAN-SLOH	504 nm (PBS)	611 nm (PBS) 667–680 nm (with Aβ monomers, oligomers and fibrils)	–	[93]
	DBAN-OSLM	521 nm (PBS)	604 nm (PBS) 650–685 nm (with Aβ monomers, oligomers and fibrils)	0.01	[93]
Curcumin derivatives	**CRANAD-2**	640 nm (PBS)	805 nm (PBS) 715 nm (with Aβ aggregates)	0.006	[105,106]
	CRANAD-6	(Does not bind to Aβ)	–	–	[107]
	CRANAD-23	(Does not bind to Aβ)	–	–	[107]
	CRANAD-54	–	~ 625 nm	–	[107]
	CRANAD-58	~ 630 nm (PBS)	~ 750 nm (PBS) 680–720 nm (with Aβ monomers, oligomers and aggregates)	–	[107]
	CRANAD-17	–	~ 600 nm (PBS) ~ 570 nm (with Aβ species)	–	[107]
	CRANAD-44	(Does not bind to Aβ)	–	0.29	[108]
	CRANAD-28	498 nm (PBS)	578 nm (PBS) 560–590 nm (with Aβ monomers and aggregates)	0.32	[108,109]
	CRANAD-3	600–610 nm (PBS)	730 nm (PBS) 650–690 nm (with Aβ monomers, oligomers and aggregates)	–	[110]
	Compound 3	618 nm (CH_2Cl_2)617–620 nm (with Aβ monomers, oligomers and aggregates)	668 nm (CH_2Cl_2) 688–697 nm (with Aβ monomers, oligomers and aggregates)	0.02	[113]
Phenothiazines	**Compound 4**	500 nm (PBS)	680 nm (PBS) 670 nm (with Aβ aggregates)	0.053	[119,120]
	PHTZ-1	495 nm (PBS)	670 nm (PBS) 615 nm (with Aβ aggregates)	0.005	[121]
	Compound 5	482 nm (PBS)	670 nm (PBS)610 nm (with Aβ aggregates)	0.004	[120]
Styrylquinolines	**Compound 6**	370 nm (PBS)	557 nm (PBS) 490 nm (with Aβ aggregates)	–	[82]
	Compounds 7	~ 480 nm (Hexane, Dioxane)	~ 550 nm (Hexane) ~ 625 nm (Dioxane) ~ 560 nm (with Aβ fibrils)	–	[122]
Crown ethers and aza crown ethers	**PiB-C**	–	490–500 nm (with Aβ aggregates)	–	[123]
	TBT	305 nm (buffer: 20 mM Tris-HCl, 150 mM NaCl, 8‰ v/v DMSO)	375 nm (with different metal ions)	–	[124,126]
	BTTA	318 nm (buffer: 20 mM Tris-HCl, 150 mM NaCl, 8‰ v/v DMSO)	386 nm (buffer: 20 mM Tris-HCl, 150 mM NaCl, 8‰ v/v DMSO, and with Cu^{2+})	0.18 *(Tris-HCl buffer)	[127]
Others	**FI**	465 nm (FI– Cu^{2+} complexes in 10 mM HEPES buffer)	518 nm (FI– Cu^{2+} complexes in 10 mM HEPES buffer)	–	[128]
	BPB	365 nm (with Aβ aggregates)	395, 500 nm (with $Aβ_{40}$ aggregates)510, 535 nm (with $Aβ_{42}$ aggregates)	–	[129]
	Compound 8	375 nm (upon Al^{3+} chelation in Tris-HCl buffer)	468 nm (upon Al^{3+} chelation in Tris-HCl buffer)	–	[130]

scaffolds related to thioflavin T, both aimed at labelling and detecting Aβ while chelating metals, increasing the binding affinity towards amyloid [129]. The incubation of BPB with $Aβ_{40}$ led to the appearance of two peaks at 395 and 500 nm, showing a strong fluorescence emission enhancement of BPB upon amyloid binding. The incubation of BPB with $Aβ_{42}$ resulted in the appearance of two peaks in the longer wavelength region, at 510 and 535 nm. These findings support that BPB can distinguish among the two forms of amyloid peptide, something of great importance due to their different role from early-stage AD in the toxicity and nucleation-tendency. Different binding abilities of the two thioflavin T analogue-moieties in BPB were found, the 2-phenylbenzothiazole moiety having a higher affinity towards Aβ as seen upon incubation with $Aβ_{40}$. *In vivo* studies using AD mouse models showed that BPB can cross BBB and detect and label amyloid plaques, emitting fluorescent radiation upon excitation with 365-nm light. As a higher plasma $Aβ_{40}/Aβ_{42}$ ratio accurately predicts the amyloid load in the brain, the detection and evaluation of amyloid peptides levels in blood could serve as a biomarker for the diagnosis of AD [30]. Related to these

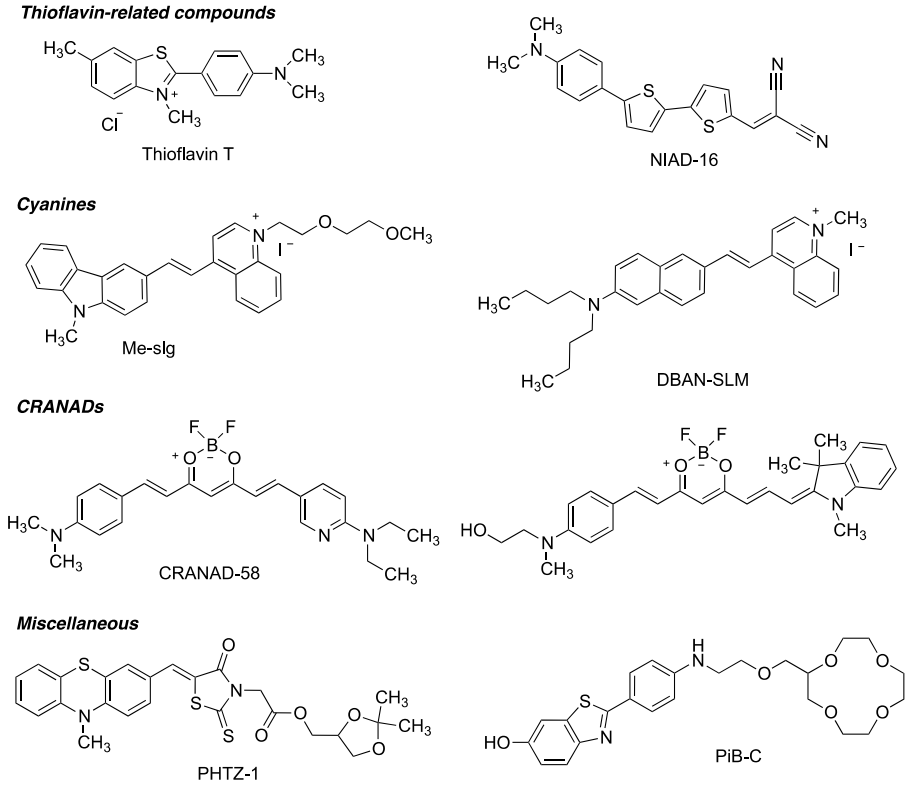

Fig. 19. Selected structures associated to theranostic properties against Alzheimer's disease.

results, the ability of BPB to detect amyloid oligomers in blood was assessed. After intravenous injection of BPB to wild-type mice and transgenic AD mice, BPB could be detected for a strong fluorescent emission at 500 nm in a blood sample from the latter but not from the former. This experiment reflected that BPB can effectively detect and label amyloid oligomers in blood and distinguish among wild-type and AD mice blood with suitable biocompatibility. *In vitro* studies with $A\beta_{40}$ solutions revealed that this compound can inhibit Zn^{2+}- and Cu^{2+}-induced Aβ aggregation and interfere with its self-aggregation; further studies showed that BPB can coordinate to Zn^{2+} and Cu^{2+} and interfere with the formation of β-sheets, thus explaining these features. BPB could also disaggregate high molecular weight amyloid aggregates into low molecular weight ones in brain homogenates of AD mice. BPB also exhibited neuroprotective effect and reduced ROS generation induced by Cu^{2+}-Aβ *in vitro*. The ability to differentiate between amyloid peptides $A\beta_{40}$ and $A\beta_{42}$ and its proved suitability to detect amyloid oligomers in mice blood make of BPB a promising theranostic tool against AD.

The biocompatible, non-fluorescent molecule **8** was designed to relief metal-involved AD pathogenesis, while providing diagnostic information due to fluorescence emission activation upon combination with Al^{3+} ions [130]. Compound **8** is highly selective and sensitive for Al^{3+} with a low detection limit, and its fluorescence turns on upon chelation with carbonyl, imine and hydroxy groups, with an excitation wavelength λ_{ex} = 375 nm and an emission maximum λ_{em} = 468 nm in Tris-HCl (50 mM, pH = 7.4) upon Al^{3+} chelation. This phenomenon does not occur with other metal ions, although **8** could form complexes with Cu^{2+}, Zn^{2+} and Fe^{3+}. Moreover, compound **8** could inhibit *in vitro* amyloid self-aggregation and Cu^{2+}-induced aggregation in similar and a stronger manner than that of curcumin, respectively, and displayed radical scavenging activity, particularly against hydroxyl radicals and superoxide radicals with a higher and lower capacity than vitamin C, respectively. Further research in living systems is needed to evaluate the suitability of **8** as a theranostic agent against AD.

6. Summary

Table 1 summarises the main therapeutic and diagnostic abilities of the compounds mentioned in this review regarding their potential application as theranostic agents against AD. Table 2 collects the optical properties of the compounds. Finally, we also summarise in Fig. 19 the main structural chemotypes that have so far yielded compounds of interest as theranostics potentially useful against Alzheimer's disease.

7. Conclusions

In the past years, many efforts have been devoted to the discovery of new diagnostic tools and therapeutic agents against AD. The combination of these efforts has yielded a number of theranostic candidates for both the diagnosis and treatment of AD. The theranostic approach represents a useful strategy considering that in AD the treatment is set too late due to difficulties achieving an early diagnosis. This type of compounds allows the assessment of the molecule activity, the organism response and the pharmacokinetics, streamlining the research process and making these compounds promising for personalized medicine. With a variety of chemical structures, ranging from cyanine, curcumin and phenothiazine derivatives to styrylquinolines, crown ethers and other diverse scaffolds, many compounds have displayed promising properties as tracers of biomarkers such as amyloid-β and showed several mechanisms to relief and counteract the different processes involved in the establishment and the development of the disease. There is no doubt that theranostics will play a key role in the discovery of new diagnostic and therapeutic resources for many medical conditions, and specifically for AD.

Declaration of competing interest

The authors declare that they have no known competing financial interests or personal relationships that could have appeared to influence

the work reported in this paper.

Data availability

No data was used for the research described in the article.

Acknowledgements

Financial support from Ministerio de Ciencia e Innovación, Spain (grant PID2021-124983OB-I00) and Ministerio de Educación y Formación Profesional, Spain (FPU fellowship FPU20/05043 to AS-V) is gratefully acknowledged.

References

[1] Z. Breijyeh, R. Karaman, Comprehensive review on Alzheimer's disease: causes and treatment, Molecules 25 (2020) 5789, https://doi.org/10.3390/molecules25245789.
[2] E. Nichols, J.D. Steinmetz, S.E. Vollset, K. Fukutaki, J. Chalek, F. Abd-Allah, A. Abdoli, A. Abualhasan, E. Abu-Gharbieh, T.T. Akram, et al., Estimation of the global prevalence of dementia in 2019 and forecasted prevalence in 2050: an analysis for the Global Burden of Disease Study 2019, Lancet Public Health 7 (2022), https://doi.org/10.1016/S2468-2667(21)00249-8 e105–e125.
[3] A.P. Porsteinsson, R.S. Isaacson, S. Knox, M.N. Sabbagh, I. Rubino, Diagnosis of early Alzheimer's disease: clinical practice in 2021, J. Prev. Alzheimers Dis. 8 (2021) 371–386, https://doi.org/10.14283/jpad.2021.23.
[4] X.X. Zhang, Y. Tian, Z.T. Wang, Y.H. Ma, L. Tan, J.T. Yu, The epidemiology of Alzheimer's disease modifiable risk factors and prevention, J. Prev. Alzheimers Dis. 8 (2021) 313–321, https://doi.org/10.14283/jpad.2021.15.
[5] C. Van Cauwenberghe, C. Van Broeckhoven, K. Sleegers, The genetic landscape of Alzheimer disease: clinical implications and perspectives, Genet. Med. 18 (2016) 421–430, https://doi.org/10.1038/gim.2015.117.
[6] J. Doroszkiewicz, B. Mroczko, New possibilities in the therapeutic approach to Alzheimer's disease, Int. J. Mol. Sci. 23 (2022) 8902, https://doi.org/10.3390/ijms23168902.
[7] J. Cummings, New approaches to symptomatic treatments for Alzheimer's disease, Mol. Neurodegener. 16 (2021) 2, https://doi.org/10.1186/s13024-021-00424-9.
[8] J. Cummings, G. Lee, P. Nahed, M.E.Z.N. Kambar, K. Zhong, J. Fonseca, K. Taghva, Alzheimer's disease drug development pipeline: 2022, Alzheimers Dement. (N Y). 8 (2022), e12295, https://doi.org/10.1002/trc2.12295.
[9] H. Rai, S. Gupta, S. Kumar, J. Yang, S.K. Singh, C. Ran, G. Modi, Near-infrared fluorescent probes as imaging and theranostic modalities for amyloid-beta and tau aggregates in Alzheimer's disease, J. Med. Chem. 65 (2022) 8550–8595, https://doi.org/10.1021/acs.jmedchem.1c01619.
[10] Y. Liu, D. Zhuang, J. Wang, H. Huang, R. Li, C. Wu, Y. Deng, G. Hu, B. Guo, Recent advances in small molecular near-infrared fluorescence probes for a targeted diagnosis of the Alzheimer disease, Analyst 147 (2022) 4701–4723, https://doi.org/10.1039/D2AN01327D.
[11] Y.I. Gyasi, Y.-P. Pang, X.-R. Li, J.-X. Gu, X.-J. Cheng, J. Liu, T. Xu, Y. Liu, Biological applications of near infrared fluorescence dye probes in monitoring Alzheimer's disease, Eur. J. Med. Chem. 187 (2020), 111982, https://doi.org/10.1016/j.ejmech.2019.111982.
[12] J. Yang, F. Zeng, Y. Ge, K. Peng, X. Li, Y. Li, Y. Xu, Development of near-infrared fluorescent probes for use in Alzheimer's disease diagnosis, Bioconjugate Chem. 31 (2020) 2–15, https://doi.org/10.1021/acs.bioconjchem.9b00695.
[13] A. Aliyan, N.P. Cook, A.A. Martí, Interrogating amyloid aggregates using fluorescent probes, Chem. Rev. 119 (2019) 11819–11856, https://doi.org/10.1021/acs.chemrev.9b00404.
[14] J. Ahmad, S. Akhter, Md Rizwanullah, M.A. Khan, L. Pigeon, R.T. Addo, N. H. Greig, P. Midoux, C. Pichon, M.A. Kamal, Nanotechnology based theranostic approaches in Alzheimer's disease management: current status and future perspective, Curr. Alzheimer Res. 14 (2017), https://doi.org/10.2174/1567205014666170508121031.
[15] A. Kumar, R.K. Chaudhary, R. Singh, S.P. Singh, S.-Y. Wang, Z.-Y. Hoe, C.-T. Pan, Y.-L. Shiue, D.-Q. Wei, A.C. Kaushik, X. Dai, Nanotheranostic applications for detection and targeting neurodegenerative diseases, Front. Neurosci. 14 (2020) 1–11, https://doi.org/10.3389/fnins.2020.00305.
[16] P. Tripathi, P. Shukla, E. Bieberich, Theranostic applications of nanomaterials in Alzheimer's disease: a multifunctional approach, Curr. Pharmaceut. Des. 28 (2022) 116–132, https://doi.org/10.2174/1381612827666211122153946.
[17] S.C. Arbor, M. Lafontaine, M. Cumbay, Amyloid-beta Alzheimer targets — protein processing, lipid rafts, and amyloid-beta pores, Yale J. Biol. Med. 89 (2016) 5–21.
[18] G.F. Chen, T.H. Xu, Y. Yan, Y.R. Zhou, Y. Jiang, K. Melcher, H.E. Xu, Amyloid beta: structure, biology and structure-based therapeutic development, Acta Pharmacol. Sin. 38 (2017) 1205–1235, https://doi.org/10.1038/aps.2017.28.
[19] M. Tolar, J. Hey, A. Power, S. Abushakra, Neurotoxic soluble amyloid oligomers drive Alzheimer's pathogenesis and represent a clinically validated target for slowing disease progression, Int. J. Mol. Sci. 22 (2021) 6355, https://doi.org/10.3390/ijms22126355.
[20] C.R. Jack, D.A. Bennett, K. Blennow, M.C. Carrillo, B. Dunn, S.B. Haeberlein, D. M. Holtzman, W. Jagust, F. Jessen, J. Karlawish, E. Liu, J.L. Molinuevo, T. Montine, C. Phelps, K.P. Rankin, C.C. Rowe, P. Scheltens, E. Siemers, H. M. Snyder, R. Sperling, C. Elliott, E. Masliah, L. Ryan, N. Silverberg, NIA-AA research framework: toward a biological definition of Alzheimer's disease, Alzheimer's Dementia 14 (2018) 535–562, https://doi.org/10.1016/j.jalz.2018.02.018.
[21] M.R. Brown, S.E. Radford, E.W. Hewitt, Modulation of β-amyloid fibril formation in Alzheimer's disease by microglia and infection, Front. Mol. Neurosci. 13 (2020), 609073, https://doi.org/10.3389/fnmol.2020.609073.
[22] L. Canevari, A.Y. Abramov, M.R. Duchen, Toxicity of amyloid β peptide: tales of calcium, mitochondria, and oxidative stress, Neurochem. Res. 29 (2004) 637–650, https://doi.org/10.1023/B:NERE.0000014834.06405.af.
[23] B. Zott, M.M. Simon, W. Hong, F. Unger, H.J. Chen-Engerer, M.P. Frosch, B. Sakmann, D.M. Walsh, A. Konnerth, A vicious cycle of β amyloid−dependent neuronal hyperactivation, Science 365 (2019) 559–565, https://doi.org/10.1126/science.aay0198.
[24] C. Haass, D. Selkoe, If amyloid drives Alzheimer disease, why have anti-amyloid therapies not yet slowed cognitive decline? PLoS Biol. 20 (2022) 1–15, https://doi.org/10.1371/journal.pbio.3001694.
[25] C. Condello, P. Yuan, A. Schain, J. Grutzendler, Microglia constitute a barrier that prevents neurotoxic protofibrillar Aβ42 hotspots around plaques, Nat. Commun. 6 (2015) 6176, https://doi.org/10.1038/ncomms7176.
[26] C. Venegas, S. Kumar, B.S. Franklin, T. Dierkes, R. Brinkschulte, D. Tejera, A. Griep, E. Gelpi, A. Vieira-saecker, S. Schwartz, F. Santarelli, P. Markus, M. Beilharz, D. Riedel, D.T. Golenbock, M. Geyer, J. Walter, E. Latz, M.T. Heneka, Microglia-derived ASC specks cross-seed amyloid-β in Alzheimer's disease, Nature 552 (2017) 355–361, https://doi.org/10.1038/nature25158.
[27] H. Hillen, The beta amyloid dysfunction (BAD) hypothesis for Alzheimer's disease, Front. Neurosci. 13 (2019) 1–10, https://doi.org/10.3389/fnins.2019.01154.
[28] J. Sinsky, K. Pichlerova, J. Hanes, Tau protein interaction partners and their roles in Alzheimer's disease and other tauopathies, Int. J. Mol. Sci. 22 (2021) 9207, https://doi.org/10.3390/ijms22179207.
[29] P. Scheltens, B. De Strooper, M. Kivipelto, H. Holstege, G. Chételat, C. E. Teunissen, J. Cummings, W.M. van der Flier, Alzheimer's disease, Lancet 397 (2021) 1577–1590, https://doi.org/10.1016/S0140-6736(20)32205-4.
[30] Y.A.R. Mahaman, K.S. Embaye, F. Huang, L. Li, F. Zhu, J.Z. Wang, R. Liu, J. Feng, X. Wang, Biomarkers used in Alzheimer's disease diagnosis, treatment, and prevention, Ageing Res. Rev. 74 (2022), https://doi.org/10.1016/j.arr.2021.101544.
[31] W.M. van Oostveen, E.C.M. de Lange, Imaging techniques in Alzheimer's disease: a review of applications in early diagnosis and longitudinal monitoring, Int. J. Mol. Sci. 22 (2021) 2110, https://doi.org/10.3390/ijms22042110.
[32] X. Xiang, K. Wind, T. Wiedemann, T. Blume, Y. Shi, N. Briel, L. Beyer, G. Biechele, F. Eckenweber, A. Zatcepin, S. Lammich, S. Ribicic, S. Tahirovic, M. Willem, M. Deussing, C. Palleis, B.S. Rauchmann, F.J. Gildehaus, S. Lindner, C. Spitz, N. Franzmeier, K. Baumann, A. Rominger, P. Bartenstein, S. Ziegler, A. Drzezga, G. Respondek, K. Buerger, R. Perneczky, J. Levin, G.U. Höglinger, J. Herms, C. Haass, M. Brendel, Microglial activation states drive glucose uptake and FDG-PET alterations in neurodegenerative diseases, Sci. Transl. Med. 13 (2021) eabe5640, https://doi.org/10.1126/scitranslmed.abe5640.
[33] H. Engler, A.F. Santillo, S.X. Wang, M. Lindau, I. Savitcheva, A. Nordberg, L. Lannfelt, B. Långström, L. Kilander, In vivo amyloid imaging with PET in frontotemporal dementia, Eur. J. Nucl. Med. Mol. Imag. 35 (2008) 100–106, https://doi.org/10.1007/s00259-007-0523-1.
[34] V.J. Lowe, B.J. Kemp, C.R. Jack, M. Senjem, S. Weigand, M. Shiung, G. Smith, D. Knopman, B. Boeve, B. Mullan, R.C. Petersen, Comparison of 18F-FDG and PiB PET in cognitive impairment, J. Nucl. Med. 50 (2009) 878–886, https://doi.org/10.2967/jnumed.108.058529.
[35] D.P. Devanand, A. Mikhno, G.H. Pelton, K. Cuasay, G. Pradhaban, J.S. Dileep Kumar, N. Upton, R. Lai, R.N. Gunn, V. Libri, Xinhua Liu, R. van Heertum, J. J. Mann, R.V. Parsey, Pittsburgh compound B (11C-PIB) and fluorodeoxyglucose (18 F-FDG) PET in patients with Alzheimer's disease, mild cognitive impairment, and healthy controls, J. Geriatr. Psychiatr. Neurol. 23 (2010) 185–198, https://doi.org/10.1177/0891988710363715.
[36] A.D. Cohen, G.D. Rabinovici, C.A. Mathis, W.J. Jagust, W.E. Klunk, M. D. Ikonomovic, Using Pittsburgh compound B for in vivo PET imaging of fibrillar amyloid-beta, Adv. Pharmacol. 64 (2012) 27–81, https://doi.org/10.1016/B978-0-12-394816-8.00002-7.
[37] S.M. Landau, C. Breault, A.D. Joshi, M. Pontecorvo, C.A. Mathis, W.J. Jagust, M. A. Mintun, Amyloid-β imaging with Pittsburgh compound B and florbetapir: comparing radiotracers and quantification methods, J. Nucl. Med. 54 (2013) 70–77, https://doi.org/10.2967/jnumed.112.109009.
[38] V. Valotassiou, J. Malamitsi, J. Papatriantafyllou, E. Dardiotis, I. Tsougos, D. Psimadas, S. Alexiou, G. Hadjigeorgiou, P. Georgoulias, SPECT and PET imaging in Alzheimer's disease, Ann. Nucl. Med. 32 (2018) 583–593, https://doi.org/10.1007/s12149-018-1292-6.
[39] W. Bao, H. Jia, S. Finnema, Z. Cai, R.E. Carson, Y.H. Huang, PET Imaging for early detection of Alzheimer's disease: from pathologic to physiologic biomarkers, Pet. Clin. 12 (2017) 329–350, https://doi.org/10.1016/j.cpet.2017.03.001.
[40] E. Morris, A. Chalkidou, A. Hammers, J. Peacock, J. Summers, S. Keevil, Diagnostic accuracy of ^{18}F amyloid PET tracers for the diagnosis of Alzheimer's disease: a systematic review and meta-analysis, Eur. J. Nucl. Med. Mol. Imag. 43 (2016) 374–385, https://doi.org/10.1007/s00259-015-3228-x.
[41] V.P. Reddy, Organofluorine compounds as positron emission tomography tracers (Chapter 7), in: V. Prakash Reddy (Ed.), Organofluorine Compounds in Biology

and Medicine, Elsevier, 2015, pp. 201–240, https://doi.org/10.1016/B978-0-444-53748-5.00007-1.
[42] J. Yang, R. Cheng, H. Fu, J. Yang, M. Kumar, J. Lu, Y. Xu, S.H. Liang, M. Cui, C. Ran, Half-curcumin analogues as PET imaging probes for amyloid beta species, Chem 55 (2019) 3630–3633, https://doi.org/10.1039/c8cc10166c.
[43] M. Maruyama, H. Shimada, T. Suhara, H. Shinotoh, B. Ji, J. Maeda, M.R. Zhang, J.Q. Trojanowski, V.M.Y. Lee, M. Ono, K. Masamoto, H. Takano, N. Sahara, N. Iwata, N. Okamura, S. Furumoto, Y. Kudo, Q. Chang, T.C. Saido, A. Takashima, J. Lewis, M.K. Jang, I. Aoki, H. Ito, M. Higuchi, Imaging of tau pathology in a tauopathy mouse model and in Alzheimer patients compared to normal controls, Neuron 79 (2013) 1094–1108, https://doi.org/10.1016/j.neuron.2013.07.037.
[44] Y. Kimura, M. Ichise, H. Ito, H. Shimada, Y. Ikoma, C. Seki, H. Takano, S. Kitamura, H. Shinotoh, K. Kawamura, M.R. Zhang, N. Sahara, T. Suhara, M. Higuchi, PET quantification of tau pathology in human brain with ^{11}C-PBB3, J. Nucl. Med. 56 (2015) 1359–1365, https://doi.org/10.2967/jnumed.115.160127.
[45] N. Okamura, T. Suemoto, S. Furumoto, M. Suzuki, H. Shimadzu, H. Akatsu, T. Yamamoto, H. Fujiwara, M. Nemoto, M. Maruyama, H. Arai, K. Yanai, T. Sawada, Y. Kudo, Quinoline and benzimidazole derivatives: candidate probes for in vivo imaging of tau pathology in Alzheimer's disease, J. Neurosci. 25 (2005) 10857–10862, https://doi.org/10.1523/JNEUROSCI.1738-05.2005.
[46] N. Okamura, S. Furumoto, R. Harada, T. Tago, T. Yoshikawa, M. Fodero-Tavoletti, R.S. Mulligan, V.L. Villemagne, H. Akatsu, T. Yamamoto, H. Arai, R. Iwata, K. Yanai, Y. Kudo, Novel ^{18}F-labeled arylquinoline derivatives for noninvasive imaging of Tau pathology in Alzheimer disease, J. Nucl. Med. 54 (2013) 1420–1427, https://doi.org/10.2967/jnumed.112.117341.
[47] N. Okamura, S. Furumoto, M.T. Fodero-Tavoletti, R.S. Mulligan, R. Harada, P. Yates, S. Pejoska, Y. Kudo, C.L. Masters, K. Yanai, C.C. Rowe, V.L. Villemagne, Non-invasive assessment of Alzheimer's disease neurofibrillary pathology using ^{18}F-THK5105 PET, Brain 137 (2014) 1762–1771, https://doi.org/10.1093/brain/awu064.
[48] R. Harada, N. Okamura, S. Furumoto, K. Furukawa, A. Ishiki, N. Tomita, K. Hiraoka, S. Watanuki, M. Shidahara, M. Miyake, Y. Ishikawa, R. Matsuda, A. Inami, T. Yoshikawa, T. Tago, Y. Funaki, R. Iwata, M. Tashiro, K. Yanai, H. Arai, Y. Kudo, [^{18}F]THK-5117 PET for assessing neurofibrillary pathology in Alzheimer's disease, Eur. J. Nucl. Med. Mol. Imag. 42 (2015) 1052–1061, https://doi.org/10.1007/s00259-015-3035-4.
[49] R. Harada, N. Okamura, S. Furumoto, K. Furukawa, A. Ishiki, N. Tomita, T. Tago, K. Hiraoka, S. Watanuki, M. Shidahara, M. Miyake, Y. Ishikawa, R. Matsuda, A. Inami, T. Yoshikawa, Y. Funaki, R. Iwata, M. Tashiro, K. Yanai, H. Arai, Y. Kudo, ^{18}F-THK5351: a novel PET radiotracer for imaging neurofibrillary pathology in Alzheimer's disease, J. Nucl. Med. 57 (2016) 208–214, https://doi.org/10.2967/jnumed.115.164848.
[50] D.W. Wooten, N.J. Guehl, E.E. Verwer, T.M. Shoup, D.L. Yokell, N. Zubcevik, N. Vasdev, R.D. Zafonte, K.A. Johnson, G. El Fakhri, M.D. Normandin, Pharmacokinetic evaluation of the tau PET radiotracer ^{18}F-T807 (^{18}F-AV-1451) in human subjects, J. Nucl. Med. 58 (2017) 484–491, https://doi.org/10.2967/jnumed.115.170910.
[51] D.T. Chien, A.K. Szardenings, S. Bahri, J.C. Walsh, F. Mu, C. Xia, W.R. Shankle, A. J. Lerner, M.Y. Su, A. Elizarov, H.C. Kolb, Early clinical PET imaging results with the novel PHF-tau radioligand [F^{18}]-T808, J. Alzheim. Dis. 38 (2014) 171–184, https://doi.org/10.3233/JAD-130098.
[52] D. Strozyk, K. Blennow, L.R. White, L.J. Launer, CSF Aβ 42 levels correlate with amyloid-neuropathology in a population-based autopsy study, Neurology 60 (2003) 652–656, https://doi.org/10.1212/01.WNL.0000046581.81650.D0.
[53] S.E. Schindler, J.G. Bollinger, V. Ovod, K.G. Mawuenyega, Y. Li, B.A. Gordon, D. M. Holtzman, J.C. Morris, T.L.S. Benzinger, C. Xiong, A.M. Fagan, R.J. Bateman, High-precision plasma β-amyloid 42/40 predicts current and future brain amyloidosis, Neurology 93 (2019) e1647–e1659, https://doi.org/10.1212/WNL.0000000000008081.
[54] K. Blennow, H. Zetterberg, Cerebrospinal fluid biomarkers for Alzheimer's disease, J. Alzheimers Dis. 18 (2009) 413–417, https://doi.org/10.3233/JAD-2009-1177.
[55] Y. Koronyo, D. Biggs, E. Barron, D.S. Boyer, J.A. Pearlman, W.J. Au, S.J. Kile, A. Blanco, D.T. Fuchs, A. Ashfaq, S. Frautschy, G.M. Cole, C.A. Miller, D. R. Hinton, S.R. Verdooner, K.L. Black, M. Koronyo-Hamaoui, Retinal amyloid pathology and proof-of-concept imaging trial in Alzheimer's disease, JCI Insight 2 (2017), https://doi.org/10.1172/JCI.INSIGHT.93621, 0–19.
[56] P.J. Snyder, J. Alber, C. Alt, L.J. Bain, B.E. Bouma, F.H. Bouwman, D.C. DeBuc, M. C.W. Campbell, M.C. Carrillo, E.Y. Chew, M.F. Cordeiro, M.R. Dueñas, B. M. Fernández, M. Koronyo-Hamaoui, C. La Morgia, R.O. Carare, S.R. Sadda, P. van Wijngaarden, H.M. Snyder, Retinal imaging in Alzheimer's and neurodegenerative diseases, Alzheimers. Dement. 17 (2021) 103–111, https://doi.org/10.1002/alz.12179.
[57] A. Kumar, J. Sidhu, A. Goyal, J.W. Tsao, Alzheimer Disease, StatPearls Publishing, Treasure Island (FL), 2023 [Updated 2022 Jun 5]. In: StatPearls [Internet].
[58] S.I. Gracon, M.J. Knapp, W.G. Berghoff, M. Pierce, R. DeJong, S.J. Lobbestael, J. Symons, S.L. Dombey, F.A. Luscombe, D. Kraemer, Safety of tacrine: clinical trials, treatment IND, and postmarketing experience, Alzheimer Dis. Assoc. Disord. 12 (1998) 93–101, https://doi.org/10.1097/00002093-199806000-00007.
[59] K.G. Yiannopoulou, S.G. Papageorgiou, Current and future treatments in Alzheimer's disease: an update, J. Cent. Nerv. Syst. Dis. 12 (2020), 117957352090739, https://doi.org/10.1177/1179573520907397.
[60] G. Khanna, R. Bhandari, A. Kuhad, A. Kuhad, Aducanumab, Drugs Future 44 (2022) 115–121, https://doi.org/10.1358/dof.2019.44.2.2895649.
[61] M. Shi, F. Chu, F. Zhu, J. Zhu, Impact of anti-amyloid-β monoclonal antibodies on the pathology and clinical profile of Alzheimer's disease: a focus on aducanumab and lecanemab, Front. Aging Neurosci. 14 (2022) 297, https://doi.org/10.3389/FNAGI.2022.870517/BIBTEX.
[62] J. Cummings, P. Aisen, C. Lemere, A. Atri, M. Sabbagh, S. Salloway, Aducanumab produced a clinically meaningful benefit in association with amyloid lowering, Alzheimer's Res. Ther. 13 (2021) 10–12, https://doi.org/10.1186/s13195-021-00838-z.
[63] R.R. Tampi, B.P. Forester, M. Agronin, Aducanumab: evidence from clinical trial data and controversies, Drugs Context 10 (2021) 2021, https://doi.org/10.7573/dic.2021-7-3, 2027-3.
[64] P. Hollmann, Update: FDA approval of Biogen's aducanumab, Geriatr. Nurs. 43 (2022) 318–319, https://doi.org/10.1016/j.gerinurse.2021.12.018.
[65] C.H. van Dyck, C.J. Swanson, P. Aisen, R.J. Bateman, C. Chen, M. Gee, M. Kanekiyo, D. Li, L. Reyderman, S. Cohen, L. Froelich, S. Katayama, M. Sabbagh, B. Vellas, D. Watson, S. Dhadda, M. Irizarry, L.D. Kramer, T. Iwatsubo, Lecanemab in early Alzheimer's disease, N. Engl. J. Med. 388 (2023) 9–21, https://doi.org/10.1056/NEJMoa2212948.
[66] E. Se Thoe, A. Fauzi, Y.Q. Tang, S. Chamyuang, A.Y.Y. Chia, A review on advances of treatment modalities for Alzheimer's disease, Life Sci. 276 (2021), 119129, https://doi.org/10.1016/j.lfs.2021.119129.
[67] M. Chakravarthy, S. Chen, P.R. Dodd, R.N. Veedu, Nucleic acid-based theranostics for tackling Alzheimer's disease, Theranostics 7 (2017) 3933–3947, https://doi.org/10.7150/thno.21529.
[68] R.K. Barr, G. Verdile, L.K. Wijaya, M. Morici, K. Taddei, V.B. Gupta, S. Pedrini, L. Jin, J.A. Nicolazzo, E. Knock, P.E. Fraser, R.N. Martins, Validation and characterization of a novel peptide that binds monomeric and aggregated β-Amyloid and inhibits the formation of neurotoxic oligomers, J. Biol. Chem. 291 (2016) 547–559, https://doi.org/10.1074/jbc.M115.679993.
[69] J. Cao, B. Zhu, K. Zheng, S. He, L. Meng, J. Song, H. Yang, Recent progress in NIR-II contrast agent for biological imaging, Front. Bioeng. Biotechnol. 7 (2020) 1–21, https://doi.org/10.3389/fbioe.2019.00487.
[70] G.P. Gellermann, K. Ullrich, A. Tannert, C. Unger, G. Habicht, S.R.N. Sauter, P. Hortschansky, U. Horn, U. Möllmann, M. Decker, J. Lehmann, M. Fändrich, Alzheimer-like plaque formation by human macrophages is reduced by fibrillation inhibitors and lovastatin, J. Mol. Biol. 360 (2006) 251–257, https://doi.org/10.1016/j.jmb.2006.05.026.
[71] W.E. Klunk, M.L. Debnath, A.M.C. Koros, J.W. Pettegrew, Chrysamine-G, a lipophilic analogue of Congo Red, inhibits Aβ-induced toxicity in PC12 cells, Life Sci. 63 (1998) 1807–1814, https://doi.org/10.1016/S0024-3205(98)00454-8.
[72] S. Aulić, M.L. Bolognesi, G. Legname, Small-molecule theranostic probes: a promising future in neurodegenerative diseases, Int. J. Cell Biol. 2013 (2013), 150952, https://doi.org/10.1155/2013/150952.
[73] E.S. Voropai, M.P. Samtsov, K.N. Kaplevskii, A.A. Maskevich, V.I. Stepuro, O. I. Povarova, I.M. Kuznetsova, K.K. Turoverov, A.L. Fink, V.N. Uversky, Spectral properties of thioflavin T and its complexes with amyloid fibrils, J. Appl. Spectrosc. 70 (2003) 868–874, https://doi.org/10.1023/B:JAPS.0000016303.37573.7e.
[74] H. Naiki, K. Higuchi, M. Hosokawa, T. Takeda, Fluorometric determination of amyloid fibrils in vitro using the fluorescent dye, thioflavine T, Anal. Biochem. 177 (1989) 244–249, https://doi.org/10.1016/0003-2697(89)90046-8.
[75] W.E. Klunk, Y. Wang, G. Feng Huang, M.L. Debnath, D.P. Holt, C.A. Mathis, Uncharged thioflavin-T derivatives bind to amyloid-beta protein with high affinity and readily enter the brain, Life Sci. 69 (2001) 1471–1484, https://doi.org/10.1016/S0024-3205(01)01232-2.
[76] C.A. Mathis, B.J. Bacskai, S.T. Kajdasz, M.E. McLellan, M.P. Frosch, B.T. Hyman, D.P. Holt, Y. Wang, G.F. Huang, M.L. Debnath, W.E. Klunk, A lipophilic thioflavin-T derivative for positron emission tomography (PET) imaging of amyloid in brain, Bioorg. Med. Chem. Lett. 12 (2002) 295–298, https://doi.org/10.1016/S0960–894X(01)00734-X.
[77] W.E. Klunk, B.J. Bacskai, C.A. Mathis, S.T. Kajdasz, M.E. McLellan, M.P. Frosch, M.L. Debnath, D.P. Holt, Y. Wang, B.T. Hyman, Imaging Aβ plaques in living transgenic mice with multiphoton microscopy and methoxy-X04, a systemically administered Congo red derivative, J. Neuropathol. Exp. Neurol. 61 (2002) 797–805, https://doi.org/10.1093/jnen/61.9.797.
[78] E.E. Nesterov, J. Skoch, B.T. Hyman, W.E. Klunk, B.J. Bacskai, T.M. Swager, In vivo optical imaging of amyloid aggregates in brain: design of fluorescent markers, Angew. Chem. Int. Ed. 44 (2005) 5452–5456, https://doi.org/10.1002/anie.200500845.
[79] S.B. Raymond, J. Skoch, I.D. Hills, E.E. Nesterov, T.M. Swager, B.J. Bacskai, Smart optical probes for near-infrared fluorescence imaging of Alzheimer's disease pathology, Eur. J. Nucl. Med. Mol. Imag. 35 (2008) 93–98, https://doi.org/10.1007/s00259-007-0708-7.
[80] N. Okamura, Styrylbenzoxazole derivatives for in vivo imaging of amyloid plaques in the brain, J. Neurosci. 24 (2004) 2535–2541, https://doi.org/10.1523/JNEUROSCI.4456-03.2004.
[81] Q. Li, J. Min, Y.H. Ahn, J. Namm, E.M. Kim, R. Lui, H.Y. Kim, Y. Ji, H. Wu, T. Wisniewski, Y.T. Chang, Styryl-based compounds as potential in vivo imaging agents for β-amyloid plaques, Chembiochem 8 (2007) 1679–1687, https://doi.org/10.1002/cbic.200700154.
[82] M. Staderini, S. Aulić, M. Bartolini, H.N.A. Tran, V. González-Ruiz, D.I. Pérez, N. Cabezas, A. Martínez, M.A. Martín, V. Andrisano, G. Legname, J.C. Menéndez, M.L. Bolognesi, A fluorescent styrylquinoline with combined therapeutic and

diagnostic activities against Alzheimer's and prion diseases, ACS Med. Chem. Lett. 4 (2013) 225–229, https://doi.org/10.1021/ml3003605.
[83] M.L. Bolognesi, A. Gandini, F. Prati, E. Uliassi, From companion diagnostics to theranostics: a new avenue for Alzheimer's disease? J. Med. Chem. 59 (2016) 7759–7770, https://doi.org/10.1021/acs.jmedchem.6b00151.
[84] W. Yang, Y. Wong, O.T.W. Ng, L.-P. Bai, D.W.J. Kwong, Y. Ke, Z.-H. Jiang, H.-W. Li, K.K.L. Yung, M.S. Wong, Inhibition of beta-amyloid peptide aggregation by multifunctional carbazole-based fluorophores, Angew. Chem. Int. Ed. 51 (2012) 1804–1810, https://doi.org/10.1002/anie.201104150.
[85] C. Chen, D. Xu, Z.-H. Zhang, S.-Z. Jia, X.-C. Cao, Y.-B. Chen, G.-L. Song, M. S. Wong, H.W. Li, Cognitive improvement and synaptic deficit attenuation by a multifunctional carbazole-based cyanine in AD mice model through regulation of Ca^{2+}/CaMKII/CREB signaling pathway, Exp. Neurol. 327 (2020), 113210, https://doi.org/10.1016/j.expneurol.2020.113210.
[86] C. Wang, X. Wang, H. Chan, G. Liu, Z. Wang, H. Li, M.S. Wong, Amyloid-β oligomer-targeted gadolinium-based NIR/MR dual-modal theranostic nanoprobe for Alzheimer's disease, Adv. Funct. Mater. 30 (2020), 1909529, https://doi.org/10.1002/adfm.201909529.
[87] Y. Li, D. Xu, A. Sun, S.-L. Ho, C.-Y. Poon, H.-N. Chan, O.T.W. Ng, K.K.L. Yung, H. Yan, H.-W. Li, M.S. Wong, Fluoro-substituted cyanine for reliable in vivo labelling of amyloid-β oligomers and neuroprotection against amyloid-β induced toxicity, Chem. Sci. 8 (2017) 8279–8284, https://doi.org/10.1039/C7SC03974C.
[88] A. Iyaswamy, X. Wang, S. Krishnamoorthi, V. Kaliamoorthy, S. G. Sreenivasmurthy, S.S. Kumar Durairajan, J.-X. Song, B.C. Tong, Z. Zhu, C.-F. Su, J. Liu, K.-H. Cheung, J.-H. Lu, J.-Q. Tan, H.-W. Li, M.S. Wong, M. Li, Theranostic F-SLOH mitigates Alzheimer's disease pathology involving TFEB and ameliorates cognitive functions in Alzheimer's disease models, Redox Biol. 51 (2022), 102280, https://doi.org/10.1016/j.redox.2022.102280.
[89] Y. Li, C. Chen, D. Xu, C.-Y. Poon, S.-L. Ho, R. Zheng, Q. Liu, G. Song, H.-W. Li, M. S. Wong, Effective theranostic cyanine for imaging of amyloid species in vivo and cognitive improvements in mouse model, ACS Omega 3 (2018) 6812–6819, https://doi.org/10.1021/acsomega.8b00475.
[90] W. Zhou, X. Hu, K.Y. Tam, Systemic clearance and brain distribution of carbazole-based cyanine compounds as Alzheimer's disease drug candidates, Sci. Rep. 7 (2017), 16368, https://doi.org/10.1038/s41598-017-16635-4.
[91] Y. Ma, Z. Ye, C. Zhang, X. Wang, H.-W. Li, M.S. Wong, H.-B. Luo, L. Xiao, Deep red blinking fluorophore for nanoscopic imaging and inhibition of β-amyloid peptide fibrillation, ACS Nano 14 (2020) 11341–11351, https://doi.org/10.1021/acsnano.0c03400.
[92] Y. Li, D. Xu, S.L. Ho, H.W. Li, R. Yang, M.S. Wong, A theranostic agent for in vivo near-infrared imaging of β-amyloid species and inhibition of β-amyloid aggregation, Biomaterials 94 (2016) 84–92, https://doi.org/10.1016/j.biomaterials.2016.03.047.
[93] X. Wang, C. Wang, H.-N. Chan, I. Ashok, S.K. Krishnamoorthi, M. Li, H.-W. Li, M. S. Wong, Amyloid-β oligomer targeted theranostic probes for in vivo NIR imaging and inhibition of self-aggregation and amyloid-β induced ROS generation, Talanta 224 (2021), 121830, https://doi.org/10.1016/j.talanta.2020.121830.
[94] Y. Li, D. Xu, H.-N. Chan, C.-Y. Poon, S.-L. Ho, H.-W. Li, M.S. Wong, Dual-modal NIR-fluorophore conjugated magnetic nanoparticle for imaging amyloid-β species in vivo, Small 14 (2018), 1800901, https://doi.org/10.1002/smll.201800901.
[95] X. Wang, H.N. Chan, N. Desbois, C.P. Gros, F. Bolze, Y. Li, H.W. Li, M.S. Wong, Multimodal theranostic cyanine-conjugated Gadolinium(III) complex for in vivo imaging of amyloid-β in an Alzheimer's disease mouse model, ACS Appl. Mater. Interfaces 13 (2021) 18525–18532, https://doi.org/10.1021/acsami.1c01585.
[96] R.M.S. Wong, H.W. Li, D.W.J. Kwong, K.K.L. Yung, Y. Ke, Novel beta-amyloid aggregate inhibitors for Alzheimer's disease, Hong Kong Med. J. 25 (2019) 26–29.
[97] H.N. Chan, D. Xu, S.L. Ho, M.S. Wong, H.W. Li, Ultra-sensitive detection of protein biomarkers for diagnosis of Alzheimer's disease, Chem. Sci. 8 (2017) 4012–4018, https://doi.org/10.1039/c6sc05615f.
[98] M. Necula, C.N. Chirita, J. Kuret, Cyanine dye N744 inhibits tau fibrillization by blocking filament extension: implications for the treatment of tauopathic neurodegenerative diseases, Biochemistry 44 (2005) 10227–10237, https://doi.org/10.1021/bi050387o.
[99] E.E. Congdon, Y.H. Figueroa, L. Wang, G. Toneva, E. Chang, J. Kuret, C. Conrad, K.E. Duff, Inhibition of tau polymerization with a cyanine dye in two distinct model systems, J. Biol. Chem. 284 (2009) 20830–20839, https://doi.org/10.1074/jbc.M109.016089.
[100] J. Gu, U.R. Anumala, R. Heyny-vonHaußen, J. Hölzer, V. Goetschy-Meyer, G. Mall, I. Hilger, C. Czech, B. Schmidt, Design, synthesis and biological evaluation of trimethine cyanine dyes as fluorescent probes for the detection of tau fibrils in Alzheimer's disease brain and olfactory epithelium, ChemMedChem 8 (2013) 891–897, https://doi.org/10.1002/cmdc.201300090.
[101] H.L. Yang, S.Q. Fang, Y.W. Tang, C. Wang, H. Luo, L.L. Qu, J.H. Zhao, C.J. Shi, F. C. Yin, X.B. Wang, L.Y. Kong, A hemicyanine derivative for near-infrared imaging of β-amyloid plaques in Alzheimer's disease, Eur. J. Med. Chem. 179 (2019) 736–743, https://doi.org/10.1016/j.ejmech.2019.07.005.
[102] H. Yang, F. Zeng, Y. Luo, C. Zheng, C. Ran, J. Yang, Curcumin scaffold as a multifunctional tool for Alzheimer's disease research, Molecules 27 (2022) 3879, https://doi.org/10.3390/molecules27123879.
[103] E.K. Ryu, Y.S. Choe, K.H. Lee, Y. Choi, B.T. Kim, Curcumin and dehydrozingerone derivatives: synthesis, radiolabeling, and evaluation for β-amyloid plaque imaging, J. Med. Chem. 49 (2006) 6111–6119, https://doi.org/10.1021/jm0607193.
[104] M. Garcia-Alloza, L.A. Borrelli, A. Rozkalne, B.T. Hyman, B.J. Bacskai, Curcumin labels amyloid pathology in vivo, disrupts existing plaques, and partially restores distorted neurites in an Alzheimer mouse model, J. Neurochem. 102 (2007) 1095–1104, https://doi.org/10.1111/j.1471-4159.2007.04613.x.
[105] R. Chongzhao, X. Xiaoyin, S.B. Raymond, B.J. Ferrara, K. Neal, B.J. Bacskai, Z. Medarova, A. Moore, Design, synthesis, and testing of difluoroboron-derivatized curcumins as near-infrared probes for in vivo detection of amyloid-β deposits, J. Am. Chem. Soc. 131 (2009) 15257–15261, https://doi.org/10.1021/ja9047043.
[106] X. Zhang, Y. Tian, Z. Li, X. Tian, H. Sun, H. Liu, A. Moore, C. Ran, Design and synthesis of curcumin analogues for in vivo fluorescence imaging and inhibiting copper-induced cross-linking of amyloid beta species in Alzheimer's disease, J. Am. Chem. Soc. 135 (2013) 16397–16409, https://doi.org/10.1021/ja405239v.
[107] X. Zhang, Y. Tian, Z. Li, X. Tian, H. Sun, H. Liu, A. Moore, C. Ran, Design and synthesis of curcumin analogues for in vivo fluorescence imaging and inhibiting copper-induced cross-linking of amyloid beta species in Alzheimer's disease, J. Am. Chem. Soc. 135 (2013) 16397–16409, https://doi.org/10.1021/ja405239v.
[108] X. Zhang, Y. Tian, P. Yuan, Y. Li, M.A. Yaseen, J. Grutzendler, A. Moore, C. Ran, A bifunctional curcumin analogue for two-photon imaging and inhibiting crosslinking of amyloid beta in Alzheimer's disease, Chem 50 (2014) 11550–11553, https://doi.org/10.1039/C4CC03731F.
[109] K. Ran, J. Yang, A.V. Nair, B. Zhu, C. Ran, CRANAD-28: a robust fluorescent compound for visualization of amyloid beta plaques, Molecules 25 (2020) 863, https://doi.org/10.3390/molecules25040863.
[110] X. Zhang, Y. Tian, C. Zhang, X. Tian, A.W. Ross, R.D. Moir, H. Sun, R.E. Tanzi, A. Moore, C. Ran, Near-infrared fluorescence molecular imaging of amyloid beta species and monitoring therapy in animal models of Alzheimer's disease, Proc. Natl. Acad. Sci. U. S. A 112 (2015) 9734–9739, https://doi.org/10.1073/pnas.1505420112.
[111] Y. Li, J. Yang, H. Liu, J. Yang, L. Du, H. Feng, Y. Tian, J. Cao, C. Ran, Tuning the stereo-hindrance of a curcumin scaffold for the selective imaging of the soluble forms of amyloid beta species, Chem. Sci. 8 (2017) 7710–7717, https://doi.org/10.1039/c7sc02050c.
[112] J. Yang, R. Cheng, H. Fu, J. Yang, M. Kumar, J. Lu, Y. Xu, S.H. Liang, M. Cui, C. Ran, Half-curcumin analogues as PET imaging probes for amyloid beta species, Chem 55 (2019) 3630–3633, https://doi.org/10.1039/c8cc10166c.
[113] D. Fang, X. Wen, Y. Wang, Y. Sun, R. An, Y. Zhou, D. Ye, H. Liu, Engineering of donor-acceptor-donor curcumin analogues as near-infrared fluorescent probes for in vivo imaging of amyloid-β species, Theranostics 12 (2022) 3178–3195, https://doi.org/10.7150/thno.68679.
[114] J. Yang, B. Zhu, W. Yin, Z. Han, C. Zheng, P. Wang, C. Ran, Differentiating Aβ40 and Aβ42 in amyloid plaques with a small molecule fluorescence probe, Chem. Sci. 11 (2020) 5238–5245, https://doi.org/10.1039/d0sc02060e.
[115] J. Yang, J. Yang, S.H. Liang, Y. Xu, A. Moore, C. Ran, Imaging hydrogen peroxide in Alzheimer's disease via cascade signal amplification, Sci. Rep. 6 (2016), 35613, https://doi.org/10.1038/srep35613.
[116] J. Yang, J. Yang, Y. Li, Y. Xu, C. Ran, Near-infrared fluorescence ocular imaging (NIRFOI) of Alzheimer's disease, Mol. Imag. Biol. 21 (2019) 35–43, https://doi.org/10.1007/s11307-018-1213-z.
[117] J. Yang, X. Zhang, P. Yuan, J. Yang, Y. Xu, J. Grutzendler, Y. Shao, A. Moore, C. Ran, Oxalate-curcumin–based probe for micro- and macroimaging of reactive oxygen species in Alzheimer's disease, Proc. Natl. Acad. Sci. U. S. A 114 (2017) 12384–12389, https://doi.org/10.1073/pnas.1706248114.
[118] J. Yang, W. Yin, R. Van, K. Yin, P. Wang, C. Zheng, B. Zhu, K. Ran, C. Zhang, M. Kumar, Y. Shao, C. Ran, Turn-on chemiluminescence probes and dual-amplification of signal for detection of amyloid beta species in vivo, Nat. Commun. 11 (2020) 4052, https://doi.org/10.1038/s41467-020-17783-4.
[119] P. Dao, F. Ye, Y. Liu, Z.Y. Du, K. Zhang, C.Z. Dong, B. Meunier, H. Chen, Development of Phenothiazine-based theranostic compounds that act both as inhibitors of β-amyloid aggregation and as imaging probes for amyloid plaques in Alzheimer's disease, ACS Chem. Neurosci. 8 (2017) 798–806, https://doi.org/10.1021/acschemneuro.6b00380.
[120] Y.L. Li, J. Cai, L. Yan, W. Zhang, L. Li, Z. Du, Y.X. Fang, C.Z. Dong, B. Meunier, H. Chen, Phenothiazine-based theranostic compounds for in vivo near-infared fluorescence imaging of β-amyloid plaques and inhibition of Aβ aggregation, Dyes Pigments 171 (2019), 107744, https://doi.org/10.1016/j.dyepig.2019.107744.
[121] Y. Li, L. Yan, J. Cai, W. Zhang, L. Li, Z. Du, C. Dong, B. Meunier, H. Chen, Development of novel theranostic agents for in vivo amyloid imaging and protective effects on human neuroblastoma cells, Eur. J. Med. Chem. 181 (2019), 111585, https://doi.org/10.1016/j.ejmech.2019.111585.
[122] M. Piquero Martí, New Multitarget Theranostic Compounds against Proteinopathies and Infectious Diseases, PhD Thesis, Universidad Complutense de Madrid, 2020 (Supervisors: P. López-Alvarado, J.C. Menéndez).
[123] Y. Tian, X. Zhang, Y. Li, T.M. Shoup, X. Teng, D.R. Elmaleh, A. Moore, C. Ran, Crown ethers attenuate aggregation of amyloid beta of Alzheimer's disease, Chem 50 (2014) 15792–15795, https://doi.org/10.1039/c4cc06029f.
[124] T. Yang, X. Wang, C. Zhang, X. Ma, K. Wang, Y. Wang, J. Luo, L. Yang, C. Yao, X. Wang, Specific self-monitoring of metal-associated amyloid-β peptide disaggregation by a fluorescent chelator, Chem 52 (2016) 2245–2248, https://doi.org/10.1039/C5CC08898D.
[125] L. Wang, Y.-L. Yin, X.-Z. Liu, P. Shen, Y.-G. Zheng, X.-R. Lan, C.-B. Lu, J.-Z. Wang, Current understanding of metal ions in the pathogenesis of Alzheimer's disease, Transl. Neurodegener. 9 (2020) 10, https://doi.org/10.1186/s40035-020-00189-z.

[126] X. Wang, X. Wang, Z. Guo, Metal-involved theranostics: an emerging strategy for fighting Alzheimer's disease, Coord. Chem. Rev. 362 (2018) 72–84, https://doi.org/10.1016/j.ccr.2018.03.010.
[127] T. Yang, L. Yang, C. Zhang, Y. Wang, X. Ma, K. Wang, J. Luo, C. Yao, X. Wang, X. Wang, A copper–amyloid-β targeted fluorescent chelator as a potential theranostic agent for Alzheimer's disease, Inorg. Chem. Front. 3 (2016) 1572–1581, https://doi.org/10.1039/C6QI00268D.
[128] B. Muthuraj, S. Layek, S.N. Balaji, V. Trivedi, P.K. Iyer, Multiple function fluorescein probe performs metal chelation, disaggregation, and modulation of aggregated Aβ and Aβ-Cu complex, ACS Chem. Neurosci. 6 (2015) 1880–1891, https://doi.org/10.1021/acschemneuro.5b00205.
[129] X. Ma, Y. Wang, J. Hua, C. Xu, T. Yang, J. Yuan, G. Chen, Z. Guo, X. Wang, A β-sheet-targeted theranostic agent for diagnosing and preventing aggregation of pathogenic peptides in Alzheimer's disease, Sci. China Chem. 63 (2020) 73–82, https://doi.org/10.1007/s11426-019-9594-y.
[130] X. Kou, X. Li, C. Hu, J. Liu, Y. Chen, Y. Zhang, A. Yang, R. Shen, Multifunctional fluorescence sensor as a potential theranostic agent against Alzheimer's disease, Spectrochim. Acta Mol. Biomol. Spectrosc. 267 (2022), 120587, https://doi.org/10.1016/j.saa.2021.120587.